RSC Advances

REVIEW

View Article Online
View Journal | View Issue

Cite this: *RSC Adv.*, 2022, **12**, 31801

ZIF-8 metal organic framework materials as a superb platform for the removal and photocatalytic degradation of organic pollutants: a review

Aicha Elaouni,†[a] M. El Ouardi,†[ab] M. Zbair,[cd] A. BaQais,[e] M. Saadi[a] and H. Ait Ahsaine*[a]

Metal organic frameworks (MOFs) are attracting significant attention for applications including adsorption, chemical sensing, gas separation, photocatalysis, electrocatalysis and catalysis. In particular, zeolitic imidazolate framework 8 (ZIF-8), which is composed of zinc ions and imidazolate ligands, have been applied in different areas of catalysis due to its outstanding structural and textural properties. It possesses a highly porous structure and chemical and thermal stability under varying reaction conditions. When used alone in the reaction medium, the ZIF-8 particles tend to agglomerate, which inhibits their removal efficiency and selectivity. This results in their mediocre reusability and separation from aqueous conditions. Thus, to overcome these drawbacks, several well-designed ZIF-8 structures have emerged by forming composites and heterostructures and doping. This review focuses on the recent advances on the use of ZIF-8 structures (doping, composites, heterostructures, *etc.*) in the removal and photodegradation of persistent organic pollutants. We focus on the adsorption and photocatalysis of three main organic pollutants (methylene blue, rhodamine B, and malachite green). Finally, the key challenges, prospects and future directions are outlined to give insights into game-changing breakthroughs in this area.

Received 10th September 2022
Accepted 24th October 2022

DOI: 10.1039/d2ra05717d

rsc.li/rsc-advances

[a]*Laboratoire de Chimie Appliquée des Matériaux, Centre des Sciences des Matériaux, Faculty of Sciences, Mohammed V University in Rabat, Morocco. E-mail: h.aitahsaine@um5r.ac.ma*

[b]*Université de Toulon, AMU, CNRS, IM2NP, CS 60584, Toulon Cedex 9, F-83041, France*

[c]*Université de Haute-Alsace, CNRS, IS2M UMR 7361, F-68100 Mulhouse, France*

[d]*Université de Strasbourg, 67081, Strasbourg, France*

[e]*Department of Chemistry, College of Science, Princess Nourah Bint Abdulrahman University, P.O. Box 84428, Riyadh 11671, Saudi Arabia*

† These authors contributed equally.

Aicha El Aouni Obtained her Bachelor's in Chemistry at the Department of Chemistry, Mohammed University in Rabat. In 2021, she obtained a Master's Degree in the valorization and characterization of rare earth materials from the Faculty of Sciences, Mohammed V University in Rabat. She is currently a PhD student in the group of Prof. Ait Ahsaine and Prof. Saadi.

Mohamed El Ouardi obtained a Bachelor's in Physics-Chemistry and Materials Analysis in 2019 at the Department of Chemistry of the Faculty of Science and Technology of Hassan II, University of Casablanca-Morocco. Currently, he is a PhD student co-supervised between the University of Toulon-France and the University Mohammed V of Rabat in Prof. Ait Ahsaine's/Prof. Saadi's group in Morocco and Prof. Arab's Group in France. His research focuses on developing materials based on oxides to study the evolution of their physicochemical properties towards the conversion of greenhouse gases (CO_2/CH_4).

1. Introduction

The increase in industrial activity and development of many key industries (agricultural, textile, and pharmaceutical) has led to serious pollution of the ecosystem. Consequently, pollutants including dyes, heavy metals, pharmaceuticals and agricultural based-chemicals have been found in water.[1–6] Accordingly, various technologies have been used for wastewater treatment to degrade or remove these persistent organic pollutants such as adsorption,[7] filtration,[8] membrane technology,[9] coagulation,[10] electrochemical oxidation[11,12] and photocatalytic degradation.[13–16] Besides, the transformation of concentrated or divided contaminants into non-toxic materials is a critical issue. Considering both energy and the economy, it is desirable to treat pollutants through adsorption or photocatalytic reactions.[17–19] Accordingly, to achieve an enhanced pollutant removal efficiency, scientists are pursuing new materials to develop adsorbents and photocatalysts.[20,21] On account of their large surface area, high crystallinity, chemical adaptability and well-tuned and defined nanometer-scale cavities, metal organic frameworks (MOFs) have been the subject of considerable scientific research as adsorbents and catalysts.[22] The structural diversity of MOFs is attributed to the presence of metal ions and bridging organic bonds, making them appealing materials for the elimination of emerging organic pollutants and toxic metals from wastewater.[23–26] The zeolite-type imidazole backbone material (ZIF) is a type of MOF having a zeolite skeleton structure, which is created upon reaction in a solvent using Co or Zn as the metal source and imidazole as the organic ligand.[27] Due to their unique characteristics, ZIFs have been employed in many fields since their first invention in 2006.[28] ZIF-8 is a member of the zeolitic imidazolate family, where the typical MOF comprised of 2-methylimidazole ligands and Zn(II) has been extensively exploited as a catalyst in diverse reactions such

Mohamed Zbair received his PhD Degree from Chouaib Doukkali University, Morocco in the framework of a European Project. He was a Postdoctoral Researcher at the University of Oulu in Finland. Currently, he is a Researcher at the Institute of Materials Sciences of Mulhouse, France. His research interests include adsorption, photocatalysis, and waste biomass valorization. Furthermore, he works on the design of different functional materials for different applications, such as energy storage and heterogeneous catalysis. Between 2016 and 2020, he was named Morocco's best researcher in the field of environment and ecology.

Amal BaQais is an Assistant Professor at Princess Nourah Bint Abdulrahman University-Riyadh-KSA (PNU), Chemistry Department. She completed her PhD Degree in 2019 under the supervision of Prof. Takanabe at King Abdullah University of Science and Technology (KAUST), Saudi Arabia. She is working on designing materials for energy conversion and storage applications. Dr Amal is currently working at the Research and Innovation Centre at the Engineering College.

Professor Mohamed Saadi received his PhD Degree from the University of Science and Technology of Lille, France in 1994. He has been a Professor at the Department of Chemistry at the Faculty of Sciences in Rabat, Mohammed V University, Morocco. He is a renowned national and African researcher in single crystals synthesis and X-ray analyses. He is a visiting professor at Valenciennes University (France), Orsay University (France) and University of Science and Technology of Lille. His research topics include crystallography, X-ray diffraction techniques, crystal structure and single-crystal synthesis.

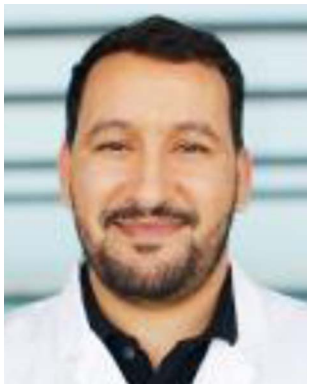

Hassan Ait Ahsaine received his BSc in Physics, MSc in Materials Chemistry from Ibn Zohr University and a co-directed PhD degree in Materials Science from Ibn Zohr University (Morocco) and Toulon University (France) in 2016. He joined the King Abdullah University of Science and Technology (KAUST) as a Postdoctoral Researcher for 2.5 years, and then was appointed as a Researcher at Mohammed VI Polytechnic University (UM6P). He is currently an Assistant Professor of Chemistry at the Mohamed V University in Rabat, Faculty of sciences. His research focuses on the development and synthesis of novel functional materials, from the nanoscale to the microscale, for environmental and catalytic applications.

as the Knoevenagel reaction,[29] photocatalytic reactions[30] and adsorption reactions.[31] ZIF-8 is also characterized by its ability to retain its crystallinity and porosity when placed in various solutions, such as water and organic solvents.[32,33] In addition, the pore size and structure of ZIF-8 are easily tunable, making it suitable for its modification.[34] Consequently, the unique chemical characteristics and physical structure of ZIF-8 offer a promising opportunity for its design and application in adsorption and photocatalytic regimes, establishing it as a hot spot for research in the removal of water pollutants.[35,36] Interestingly, ZIF-8 demonstrates great thermal stability owing to its unique structure, consisting of Zn bound to imidazolate linkers. Yaghi's group reported the preparation of a stable ZIF-8 MOF at 550 °C in a nitrogen atmosphere, which exhibited structural stability for 7 days in boiling water. The prepared ZIF-8 also maintained the same crystallinity and porosity after being placed in various organic solvents and water.[33,37,38] Similarly, Butova and coworkers reported the great thermal stability of a ZIF MOF (400 °C in air and 470 °C in N_2) in water.[39] Other studies showed that ZIF-8 prepared *via* a rapid sonochemical synthesis exhibited comparable thermal and structural stability with that prepared by conventional methods, requiring 1 day for their preparation.[40]

However, ZIF-8 presents some drawbacks such as aggregation of its nanoparticles (NPs) in water, which leads to an increase in its particle size, and therefore increased charge transfer resistance and reduction in its interfacial area, thereby reducing its adsorption ability.[41] Furthermore, due to its wide band gap, ZIF-8 has low reactivity under visible light, and consequently its photo-activity cannot reach the same degree of traditional semiconductors.[42] Regarding their separation and recyclability, the separation of ZIF-8 NPs from the reaction medium and their reusability are difficult. In addition, the need for hybrid materials in various applications has rendered the application of pure ZIF-8 very limited.[43] Thus, to overcome these limitations, some modifications have been performed, for example, the controllable association of ZIF-8 with other materials to widen its light adsorption region and to reduce the aggregation of its particles, thus guaranteeing a better adsorption and photocatalysis performance.[44,45] Thus far, ZIF-8 hybrids have been successfully developed, together with active materials, such as carbon nanotubes, metals, oxides, polymers, fibers, and metal NPs.[46] Compared to pristine ZIF-8, ZIF-8 hybrid materials not only have improved adsorption ability with the photocatalytic efficiency of ZIF-8, but have also expanded the scope of application of ZIF-8. Lately, several research projects have confirmed the validity of this combination strategy. For example, the combination of ZIF-8 with ZnO resulted in molecule size selectivity and excellent photocatalytic efficiency.[47,48] Similarly, a ZIF-8@TiO_2 composite demonstrated enhanced efficiency for the degradation of rhodamine B (RhB).[49] The fibers formed by a combination of ZIF-8 with polydopamine and poly-acrylonitrile (ZIF-8@PDA/PAN) showed good flexibility and easy separation from the reactive medium after the adsorption process.[50] Compared to both neat ZIF-8 and MoO_3 nanowires, the ZIF-8/MoO_3 composite exhibited a higher photocatalytic ability towards the reduction of chromium(VI).[51]

Thus far, many articles and reviews have discussed the different strategies for the synthesis of MOFs and their physicochemical properties.[52,53] Nevertheless, there are limited reviews focusing on the application of ZIF-8 hybrids in the photocatalysis and adsorption of water pollutants. Thus, in this review, we discuss the recent progress of ZIF-8-based hybrids in the adsorption and photodegradation of wastewater contaminants (Fig. 1), with the evaluation of some representatives.

2. ZIF-8-based materials for the removal of organic pollutants

Owing to its unique chemical and physical properties, the ZIF-8 MOF is generally implemented to effectively eliminate many types of pollutants from wastewater as both an adsorbent and photocatalyst.[48,54–58] ZIF-8 MOFs can be synthesized using different solvents and solvent-free methods including solvothermal, hydrothermal, ionothermal, sonochemical, accelerating agent, mechanochemical and direct solvent-free procedures.[15] Their synthesis is dependent on specific catalytic reaction conditions. For instance, solvent-free synthesis leads to the formation of multi-variate ZIF materials and their pores are not partially covered by organic solvents. However, in most cases, the orientation of the metal coordination polyhedra can led to new zeolitic topologies with have high thermal and chemical stability.

Nevertheless, ZIF-8 exhibits low recyclability and its specific surface areas considerably decreases due to the aggregation and the packing of its particles.[59] Consequently, the construction of ZIF-8-based composites has been proposed to address these problems. Thus, successful synthesis strategies were employed to strengthen the ZIF-8 MOF in wastewater purification[60–62]

In the following subchapters, we review the current advances in the use of ZIF-8-based materials as adsorbents for the

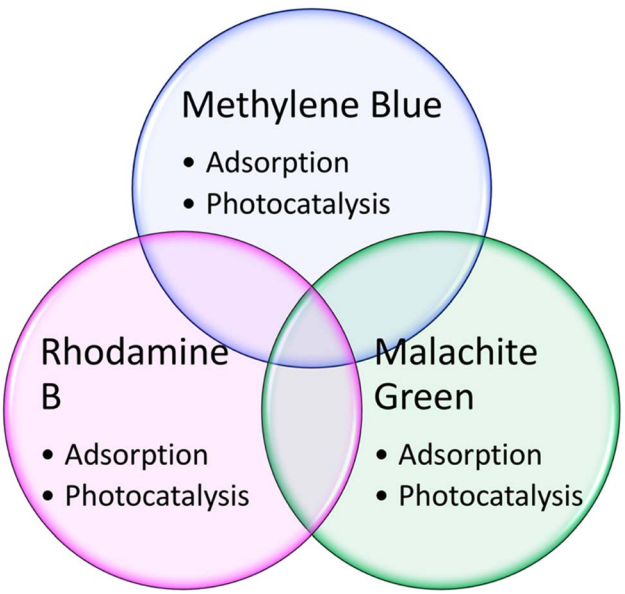

Fig. 1 Three model pollutants discussed herein using ZIF-8 structures.

removal of various pollutants from wastewater, focusing on three main organic pollutants (methylene blue (MB), rhodamine B (RhB), and malachite green (MG)).

2.1 ZIF-8 hybrid structures

Adsorption is the most appropriate and promising method for the removal of several contaminants because of its simplicity, low cost, and excellent performance. The adsorption process efficiency is influenced by many factors such as the nature of the adsorbent, the type of pollutant and type interactions occurring between the sorbent and adsorbate.[63–67] Compared with the traditional and commercially available adsorbent materials, including coconut shells, layered double hydroxides (LDH), and activated carbon, ZIF-8-based materials possess high porosity and a large specific surface area, endowing this type of material the ability to adsorb several molecules with various sizes.[68–70] The specific surface area determined for pure ZIF-8 nanoparticles varies between 1500 and 2500 $m^2\ g^{-1}$, which is superior to that of other adsorbents.[59,71] Alternatively, in comparison with pristine ZIF-8, ZIF-8 hybrids have shown satisfactory results for the adsorption of organic pollutants owing to their high adsorption capacity and better stability and recyclability.[72–74] Also, the synthesis of hybrid systems based on ZIF-8 prevents the aggregation of the adsorbent and facilitates its separation from water.[75,76] Various ZIF-8 hybrid materials have been reported for the removal and photocatalytic degradation of several pollutants in aqueous conditions. For instance, the removal of organic dye pollutants (*i.e.*, MB, RhB, MG) was studied in many reports using ZIF-8 materials.[54,74]

2.1.1 Adsorption of MB. Zheng *et al.*[77] successfully developed an Fe_3O_4/ZIF-8 core–shell heterostructure for the adsorption of methylene blue. The developed hybrid (Fe_3O_4/ZIF-8) showed a great specific surface area of about 1068 $m^2\ g^{-1}$ with a microporous volume of 0.39 $cm^3\ g^{-1}$, achieving a methylene blue adsorption capacity of 20.2 mg g^{-1}. Additionally, due to the excellent magnetic characteristics of the Fe_3O_4/ZIF-8 composite caused by the addition of Fe_3O_4 magnetite, the adsorbent (Fe_3O_4/ZIF-8) could be easily separated from the reaction medium and exhibited good recyclability. Alternatively, Wu *et al.*[78] successfully incorporated nucleotides molecules in an imidazolate zeolite framework called ZIF-8 (NZIF) (Fig. 2). Based on the morphological analysis, the incorporation process resulted in the formation of a hierarchical porous structure, which could remove several organic dyes, including methylene blue.

The adsorption capacity achieved by the NZIF composite for MB was 10 mg g^{-1}, which was 5-fold greater than that of pure ZIF-8. This enhancement was explained by the mesoporous nature of NZIF, which supplied more interaction sites; moreover, the adsorption mechanism investigation revealed that the adsorption capacity of NZIF mainly resulted from the hydrogen bonding and π–π stacking between the incorporated nucleotide monophosphate and the captured molecules. Alternatively, it was found that the inserted nucleoside monophosphate allowed NZIF to preserve its morphology and adsorption capacity after the adsorption process under acidic conditions, while ZIF-8 collapsed. Zhan *et al.*[79] employed the electrospinning technique and a solution containing poly-acrylonitrile (PAN) and 2-methylimidazole to fabricate a composite based on ZIF-8/PAN. The pH and temperature effect were examined to evaluate the performance of the ZIF-8/PAN composite for the adsorption of methylene blue. The authors showed that with an increase in pH to a basic value (11), the adsorption capacity was substantially enhanced, reaching 120.48 mg g^{-1}. This increase

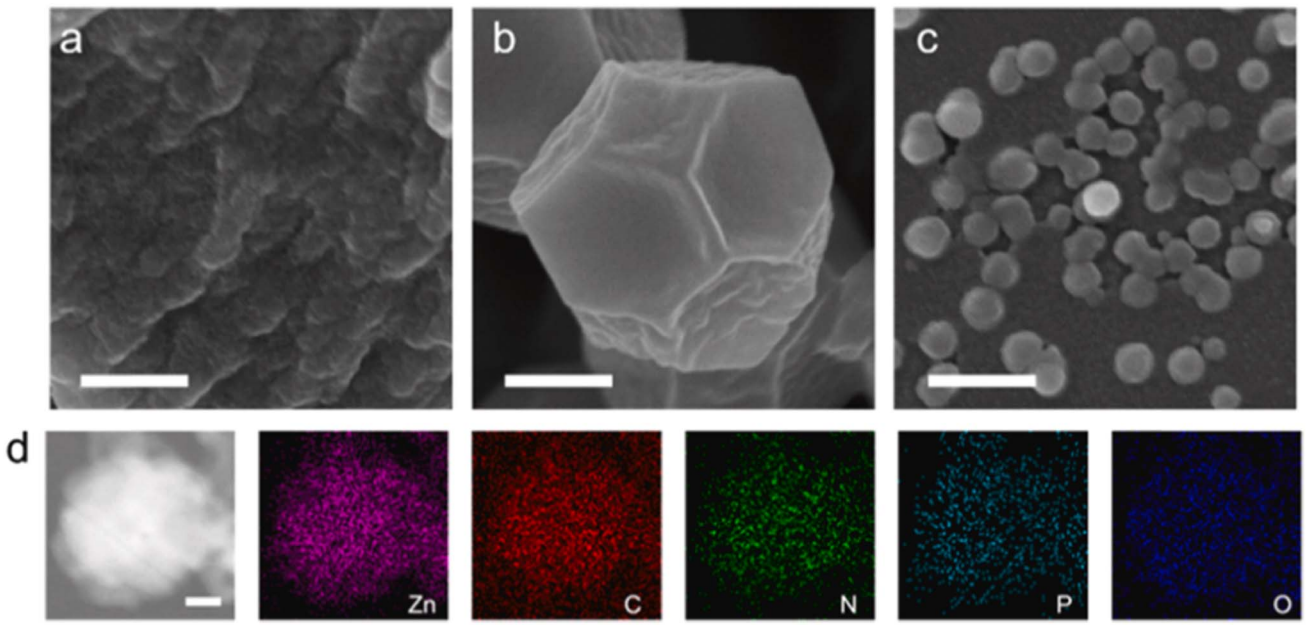

Fig. 2 SEM images of ZnAMP (a), ZIF-8 (b) and NZIF (c) (scale bar is 200 nm). (d) HAADF image of NZIF and EDS mapping of Zn, C, N, P and O, where P and O are exclusive to the nucleotide (scale bar is 20 nm). Reproduced with permission from ref. 78 Copyright ©2021, Elsevier.

in adsorption capacity was attributed to the negative zeta potential value of ZIF-8 at pH = 11, where the cationic nature of methylene blue allowed great attraction between the adsorbent (ZIF-8/PAN) and the adsorbate (MB). Conversely, the adsorption capacity decreased with an increase in temperature, which was due to the fact that an increase in temperature sped up the rate of migration of MB, also boosting the desorption rate. The results of the kinetic study showed that the adsorption of MB obeyed the pseudo-second order kinetic equation; moreover, the adsorption process implied chemical interactions among MB and ZIF-8/PAN polar functional groups. The recyclability tests proved that the adsorption capacity for MB remained higher than 85% after three cycles of regeneration in comparison with the first time.[79] In another study, Marsiezade *et al.*[80] developed a composite based on hollow beads containing carboxymethyl-cellulose, ZSM-5 and ZIF-8 (CMC/ZSM-5/ZIF-8) to remove the organic dye methylene blue. Two adsorption modes were evaluated (continuous and discontinuous). The adsorption capacities recorded for both adsorption modes (continuous and discontinuous) for CMC, CMC/ZIF-8, CMC/ZSM-5 and CMC/ZSM-5/ZIF-8 were 10.56 and 12.01, 11.87 and 13.06, 9.29 and 11.53, 8.15 and 10.49, respectively. It is well noted that ZIF-8 exhibited a positive effect compared to ZSM, which had a negative effect on the methylene blue adsorption process. They found that the adsorption of methylene blue was predominantly assigned to the CMC functional groups, which played an extensive role in the adsorption of MB as active sites for the subsequent attachment of MB molecules either by hydrogen bonding or electrostatic interaction. Furthermore, due to the presence of π electrons in the methylene blue molecule, it is advantageous for this molecule to interact with the aromatic rings in the beads by π–π stacking. Alternatively, the creation of an ionic bond between Zn^{2+} (ZIF-8) and $-SO_3^-$ (MB) played a major role in the adsorption of methylene blue on ZIF-8. The regeneration of this material was successfully evaluated in five steps, suggesting the recyclability of the composite.[80] Recently, Abdelhamid *et al.*[81] reported the growth of ZIF-8 crystal on biopolymers such as cellulose (celloZIF-8). The resulting cello/ZIF-8 materials were employed for the adsorption of methylene blue. In this work, the authors showed that the engineered cello-ZIF-8 synergistically coupled the mechanisms of pore structure adsorption, charge specific adsorption and catalytic hydrogenation, and also the addition of cellulose provided negative functional groups (COOH and OH), creating effective sites for the adsorption of methylene blue. The developed cello-ZIF-8 materials exhibited excellent recyclability during 5 cycles with no appreciable loss in their efficiencies.[81] Zhu and co-authors[82] confirmed the benefit of adding cellulose to the ZIF-8 framework to prevent the aggregation of the ZIF-8 particles. Furthermore, they showed that the fibrous ZIF-8 aerogels also combined the hierarchical porosities and low density of cellulose aerogels, and hence this combination resulted in improved adsorption capacity and kinetics. Similarly, Zhang *et al.*[83] successfully introduced their developed hybrid (ZIF-8/C_3N_4) in an agar aerogel, creating a flexible and effective aerogel adsorbent for the elimination of methylene blue from the reaction medium. This ZIF-8/C_3N_4 composite aerogel displayed an adsorption capacity of 154.87 mg g^{-1}, which was 1.44-times higher than that of the pristine ZIF-8. They explained that this improvement was due to the synergistic effect of carbon nitride (C_3N_4), which contributed to the regulation of the ZIF-8 crystal growth, leading to small and highly dispersed ZIF-8, resulting in a better performance for the removal of MB. Besides controlling the growth of ZIF-8 crystals, C_3N_4 also provided the hybrid aerogel (ZIF-8/C_3N_4) with stable repeatability for over 5 consecutive cycles. Alternatively, Zong *et al.*[84] reported the synthesis of ZIF-8 hybrid aerogels, which were produced by growing MOF crystals on aramid-nanofibril (ANF) aerogels. They indicated that the ANF/ZIF-8 hybrid aerogels showed a better adsorption capacity for cationic dyes such as methylene blue rather than anionic dyes (methyl orange), which implies that the mechanism responsible for the adsorption operation is electrostatic attractions between the formed aerogels and the dye (MB). Moreover, the high surface area, synergistic effect created between the 3D polyhedra of ANF and ZIF-8 also contributed to the adsorption of MB. Li *et al.*[85] exploited a family of transition metal-carbide-carbonitride materials (MXenes) for the development of an MXene/ZIF-8-based hybrid aerogel, which was subsequently used for the adsorption of methylene blue. The prepared composite (MXene/ZIF-8) showed a methylene blue adsorption capacity of 459 mg g^{-1}, while that of MXene alone was 286 mg g^{-1}. This capacity decreased in an acidic environment due to the elevated concentration of H^+ ions together with the cationic dyes competing for the adsorption sites, thus hindering the adsorption process. Due to the increase in temperature, the adsorbate mobility also increased, followed by an increase in the rate of diffusion of the adsorbent, where the adsorption capacity of the MXene/ZIF-8 aerogels reached the maximum value. Furthermore, the consistency of the R^2 values with the pseudo-second order model compared to the pseudo-first order model suggests that the adsorption of MB on all the MXene/ZIF-8 aerogels follows chemisorption, especially the MXene/ZIF-8-4 aerogel prepared at an MXene mass ratio of 74.2%. The reusability of MXene/ZIF-8 was studied for up to 8 cycles of desorption/regeneration, which indicated the great stability of the developed composite. After eight cycles, the adsorption capacity diminished slightly to 95.8% compared to the pristine adsorbent.[85] Similarly, Gu *et al.*[86] reported the preparation of a composite adsorbent based on an MXene ($Ti_3C_2T_x$) and ZIF-8 for the uptake of methylene blue (MB) (Fig. 3).

Due to the appropriate interstitial space arising from the ZIF-8 arrays in the MXene ($Ti_3C_2T_x$) interlayer as well as the ability of $Ti_3C_2T_x$ to capture cationic dyes such as MB, an adsorption capacity of 107 mg g^{-1} was obtained by the hybrid ZIF-8/$Ti_3C_2T_x$, which was superior to that of ZIF-8 (3 mg g^{-1}) and $Ti_3C_2T_x$ (9 mg g^{-1}). The low adsorption capacity of $Ti_3C_2T_x$ was explained by the absence of oxygen groups on its surface and inadequate internal interspace. The addition of ZIF-8 on $Ti_3C_2T_x$ provided a useful interspace, which was created by the arrangement of a small amount of ZIF-8 inside the interlayer of the MXene ($Ti_3C_2T_x$), which improved the ability to absorb methylene blue. In contrast, excess ZIF-8 had a negative effect on the adsorption ability of MB. In another work, Li *et al.*[87]

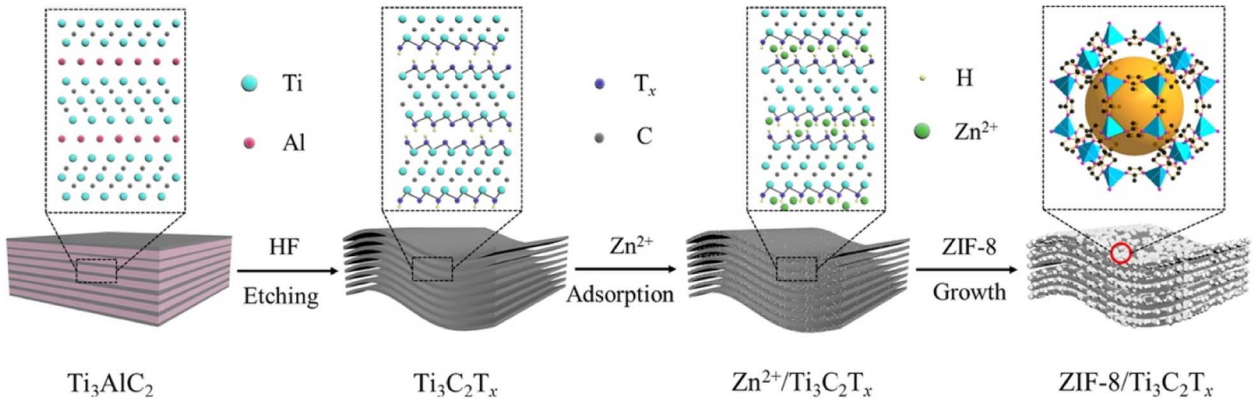

Fig. 3 Illustration of the synthesis of ZIF-8/$Ti_3C_2T_x$. Reproduced with permission from ref. 86 Copyright ©2022, Elsevier.

reported another strategy involving the introduction of a family of polyoxometalates (POM) in zeolitic-imidazolate frameworks (ZIF-8) *via* a mechano-chemical procedure at room temperature. In this study, they evaluated three different hybrids, *i.e.*, $H_3PW_{12}O_{40}$: ZIF-8 (BIT-1), $H_4SiW_{12}O_{40}$: ZIF-8 (BIT-2) and $H_3PMo_{12}O_{40}$: ZIF-8 (BIT-3), for the adsorption of methylene blue. The easy deprotonation of these composites resulted in the formation of poly-anions, which showed great ability to attract methylene blue molecules due to their cationic nature, which led to an increase the affinity of MB particles, and therefore enhanced the adsorption capacity. In addition, these composites served as open hydrophobic conduits, allowing the methylene blue molecules to diffuse inside and outside the POM/ZIF-8 composite. Moreover, the introduction of these POMs in the ZIF-8s generated a synergistic effect and increased the porosity, which resulted in excellent performances compared to ZIF-8. It has been well documented that the maximum adsorption capacity was obtained by the BIT-1 composite (810 mg g^{-1}). Compared to other adsorbents such as activated carbon and pure ZIF-8, the BIT-1 hybrid showed an outstanding efficiency, resulting in the removal of 99% methylene blue (60 ppm) within 5 min. In addition, BIT-1 also showed excellent repeatability without losing its properties such as adsorption capacity.[87]

2.1.2 Adsorption of RhB. Besides the adsorption of methylene blue, other investigations have been performed to evaluate the potential of ZIF-8-based materials to adsorb rhodamine B (RhB). In this context, Meng *et al.*[88] reported the use of a cellulosic polymer (corn-cobs) as a support to embed *in situ* Ag nanoparticle-decorated ZIF-8 nano-hybrids for the fabrication of multifunctional bio-sorbents having robust adsorption-catalytic behavior. The results indicated that the porous corncob-supported ZIF-8 decorated with Ag NPs (Ag NPs@ZIF-8/P-OCB) yielded outstanding efficiencies regarding the removal of RhB. Alternatively, the specific surface area measurements indicated that after the addition of silver nanoparticles (Ag NPs), a slight decrease in the specific surface area of the bio-adsorbent (Ag NPs@ZIF-8/P-OCBs: 224.50 m^2 g^{-1}) in comparison with the hybrids (ZIF-8s/P-OCBs: 292 m^2 g^{-1}) occurred. This decrease was explained by the great dispersion of the Ag nanoparticles, which blocked the cavities of ZIF-8. Furthermore, the adsorption capacity of RhB for both samples Ag NPs@ZIF-8/P-OCBs and (ZIF-8/P-OCBs) was 11.7 mg g^{-1} and 12.2 mg g^{-1}, respectively, which was consistent with the specific surface measurements. Specifically, the charge of the porous ZIF-8 may have enhanced the adsorption performance of P-OCB, while the addition of silver nanoparticles and their strong dispersion helped to lock the cavities of ZIF-8. Alternatively, Nasser Abdelhamid *et al.*[81] reported the growth of ZIF-8 crystal on biopolymers such as cellulose (celloZIF-8). In this work, they showed that the addition of cellulose also provided negative functional groups (COOH and OH), which could provide effective sites for the adsorption of RhB. In addition, the developed cello-ZIF-8s synergistically coupled the adsorption mechanisms of the ZIF-8 porous structure, resulting in charge specific adsorption and catalytic hydrogenation. In another work, Fan *et al.*[89] presented a new approach of exploiting ionic liquids and zeolite frameworks for the formation of hybrid systems capable of adsorbing the cationic dye RhB. In this work, the hetero-polyanion-based guanidinium ionic liquids (HPAILs) not only functioned as greener agents to effectively monitor the nucleation and growth rate of ZIF-8s, but were also embedded as a shell material for the creation of specific adsorption sites. The formed HPAIL@mesoporousZIF-8 hybrid displayed a high RhB adsorption ability of 278 mg g^{-1} and effectively eliminated 99% of RhB over a period of 15 min with pseudo-second-order kinetics. These exceptional results were ascribed to the presence of mesopores inside ZIF-8, which facilitated the diffusion of RhB. Moreover, the addition of guanidinium ionic liquid was instrumental in improving the adsorption affinity by providing additional adsorption sites. The Langmuir-isotherm model indicated that the adsorption of RhB was monolayer over a surface containing homogeneous bonding sites. Furthermore, the presence of imidazole rings, tungstate, phosphate and amino groups on the surface of the HPAIL@Meso-ZIF-8 composite suggested that the adsorption of RhB was through a variety of interactions including electrostatic interaction, van der Waals interaction and hydrogen bonding (Fig. 4). In the reuse experiments, it was found that HPAIL@Meso-ZIF-8 could

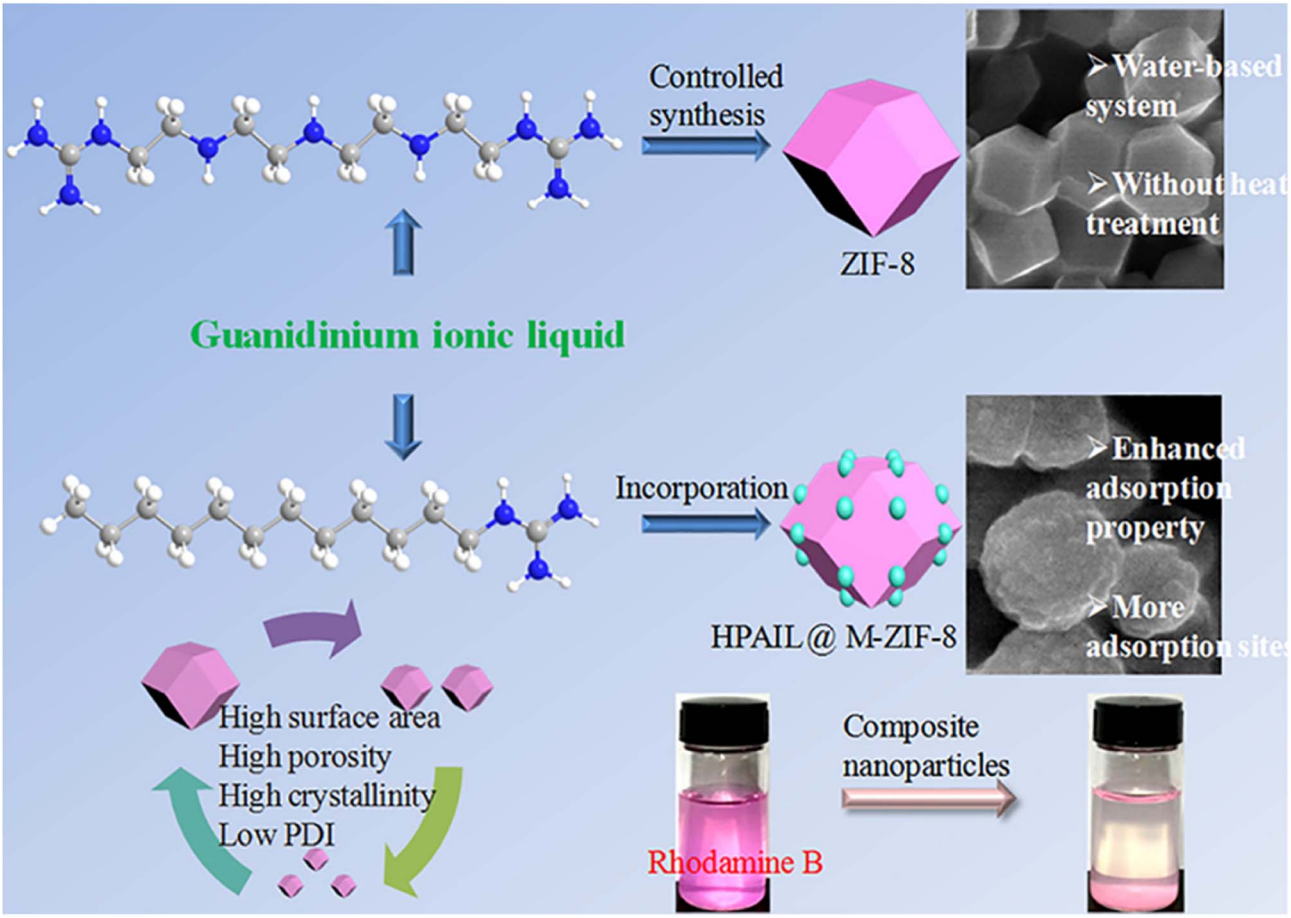

Fig. 4 HPAIL@Meso-ZIF-8 composite for the removal of RhB dye. Reproduced with permission from ref. 89 Copyright ©2022, Elsevier.

be reused for 4 cycles without losing its structural properties and adsorption performance.[89]

Chen *et al.*[90] developed a new strategy based on the use of ZIF-8s as a stabilizer for slurry polymerization from hexadecyl acrylate (AA16) in water for the successful preparation of PAA16/ZIF-8 composites, which were employed for the removal of RhB. The UV visible analysis showed that the concentration of RhB decreased by about 24%, 25% and 99% in the presence of PAA16, ZIF-8/PAA16 and ZIF-8, respectively. These results were explained by the BET analysis, which showed that the specific surface area of PAA16/ZIF-8 was about 8 $m^2 g^{-1}$, while that of ZIF-8 alone was 1745 $m^2 g^{-1}$. This large difference was attributed to the low content of ZIF-8s in the surface of PAA16, which implies that the adsorption capacity of RhB is mainly dependent on the content of ZIF-8. The reuse results showed that PAA16/ZIF-8 could be reused for 3 cycles without losing its structural properties and adsorption performance.[90] Yin *et al.*[91] employed an *in situ* method and layer-by-layer assembling method with no solvent for the growth of ZIF-8 sheets on carbon fiber (CF) tissues functionalized with carboxyl groups (–COOH). The developed ZIF-8/CF composite was employed for the adsorption of RhB. The calculated specific surface area for ZIF-8s alone was 865.764 $m^2 g^{-1}$, while that of the ZIF-8/CF composite was 495.297 $m^2 g^{-1}$. This reduction in size was attributed to the non-porous nature of CFs, whereas the HK method showed that ZIF-8s and ZIF-8/CF displayed a similar type and size of microspores, which suggests that the introduction of CF tissue did not alter did not alter the structure and pore size of ZIF-8s in the CF-ZIF-8 hybrid. Although the surface charge of the ZIF-8/CF composite was negative (−2.35 mV), the visible UV analysis showed a slower decrease in the absorption of cationic RhB, which was explained by the high molecular size of RhB. Alternatively, they found that RB19 (anionic dye) and RhB presented a similar UV reduction after the adsorption operation, which was attributed to the similarity in the π–π interaction between the CF-ZIF-8 composite and each dye. The reusability tests revealed that during 5 cycles of reuse, the adsorption capacity of the ZIF-8/CF composite showed only a slight decrease, indicating the outstanding reusability of the ZIF-8/CF hybrid.[91] Recently, Yang *et al.*[92] developed an iron-doped ZIF-8 adsorbent (Fe-ZIF-8) for the removal of several pollutants such as rhodamine B. The composite prepared at a temperature of 500 °C (Fe-ZIF-8-500) presented a specific surface area of 1135 $m^2 g^{-1}$, while the Fe-ZIF-8 sample prepared without thermal activation presented a specific surface area of 1536 $m^2 g^{-1}$. This large difference was due to the collapse of the pore channels during high temperature processing. At a pH above the pH at the zero point of charge (pH_{ZPC} = 7.53), the

surface of the composite (Fe-ZIF-8-500) was negatively charged, and due the cationic nature of RhB, an adsorption capacity of 74 mg g^{-1} was obtained. Zhang and co-authors tested the combination between two metal organic frameworks such as ZIF-8 and UiO-66-NH_2 for the removal of several organic dyes such as RhB. Compared to the removal of methylene blue on the ZIF-8/UiO-66-NH_2 composite described in this study, which demonstrated both outstanding selectivity and strong performance, despite the cationic nature of RhB, the ZIF-8-loaded UiO-66-NH_2 showed a poor adsorption efficiency for RhB. These results were explained based on the complex structure and large molecular size of RhB compared to that of MB, which could prevent it from penetrating the pores in the ZIF-8-loaded UiO-66-NH_2. Specifically, this composite had an insufficient width of 0.5 nm, while the molecule size of RhB was 1.41 × 0.98 nm. Hou *et al.*[93] reported the fabrication of a hybrid based on ZIF-8 and graphene aerogels (ZIF-8/GAs) through a counter diffusion process. Due to the unique integrated characteristics of ZIF-8s and GAs such as large surface area, great interaction between ZIF-8/GA hybrid and analytes and porous structure, the ZIF-8/GA hybrid exhibited an adsorption capacity for RhB of 320.6 mg g^{-1}, while that for GAs was 194.2 mg g^{-1}. The pseudo-second-order model had greater applicability compared to the pseudo-first-order model in describing the adsorption pathway due to its R^2 correlation coefficient of 0.999, whereas that for the pseudo-first-order model was 0.9561.[93]

2.1.3 Adsorption of organic dye malachite green. Despite its high demand in several sectors and fields such as the textile industry, aquaculture and hatchery industry, the use of malachite green (MG) and other dyes (MB and RhB) is not recommended because they have carcinogenic and mutagenic effects on human health.[94–96] To date, many reports have been published on the removal of malachite green from aqueous media using ZIF-8-based materials. For example, Zhao *et al.*[73] assembled ZIF-8s on g-C_3N_4/Fe_3O_4 to produce ZIF-8/g-C_3N_4/Fe_3O_4 nanocomposites, which were effective for adsorbing varying concentrations of malachite green. Owing to the synergistic effect of the developed ZIF-8/g-C_3N_4/Fe_3O_4 hybrid, which combined the high specific surface area of ZIF-8, the unique structure of g-C_3N_4 and the superparamagnetic characteristics of Fe_3O_4, it exhibited an outstanding uptake ability of about 3412 mg g^{-1}. Moreover, due to its easy separation from the reaction medium, the hybrid could be used repeatedly after five cycles without loss in its structural properties and adsorption performance. They found that the increase in pH was advantageous for the adsorption of MG because the surface of the ZIF-8/g-C_3N_4/Fe_3O_4 composite becomes negative, which causes an electrostatic interaction with green malachite because it is cationic in nature. Alternatively, the infrared analysis carried out before and after the adsorption operation demonstrated the existence of an H-bond between MG and ZIF-8/g-C_3N_4/Fe_3O_4 as well as the appearance of a π–π stacking effect between MG and the ZIF-8/g-C_3N_4/Fe_3O_4. The pseudo-second-order model was more applicable compared to the pseudo-first-order model in describing the adsorption pathway due to its R^2 correlation coefficient of 0.999 compared to that of the pseudo-first-order model of 0.813.[73] Zadvarzi *et al.*[97] reported the fabrication of a magnetic chitosan (chitosan@Fe_3O_4) coated with ZIF-8 for the removal of the cationic dye malachite green. In this work, several parameters were studied to improve the performance of the ZIF-8@chitosan@Fe_3O_4 hybrid for the efficient adsorption of MG, and the optimal conditions were found to be 40 mg of adsorbent, pH = 7, 10 ppm initial concentration, a temperature of 25 °C and 40 min reaction time. It was noted that the equilibrium data obtained were in good accordance with the Langmuir model with a maximum capacity of 3.282 mg g^{-1}. The theoretical study based on first principles calculation revealed that there was no meaningful interaction between MG and Fe_3O_4 as well as with chitosan, and hence the only interaction existed was that between ZIF-8 and MG. Moreover, the lowest adsorption energy value and long bonding distances indicated that the adsorption of MG was according to van der Waals forces, confirming the occurrence physisorption.[97] Mahmoodi *et al.*[74] successfully deposited ZIF-8 crystals on chitosan/polyvinyl-alcohol electrospun nanofibers (ZIF-8-CS/PVA-ENF) to eliminate malachite green from aqueous medium. An enhancement in the effective surface area and porosity was observed after the successful synthesis of ZIF-8 applied on CS/PVA for the second cycle (ZIF-8-CS/PVA-ENF2), and the characterization images of each material are displayed in Fig. 5. It is obvious that the composite prepared in the second cycle (ZIF-8-CS/PVA-ENF2) presented better performances towards the removal of MG, and the adsorption ability of MG was 1000 mg g^{-1} with high repeatability and stability of 90%. The suggested adsorption mechanism for this study is presented in Fig. 5e, where two types of interactions were discussed such as the electrostatic attraction due to the negative charge on the surface of the material (ZIF-8-CS/PVA-ENF2) and the cationic nature of MG. The second interaction is the π–π attraction between the benzene structures, which are comprised of π-bonds in ZIF-8-CS/PVA-ENF2, and the dye molecules.[74] In another work, composite hollow microspheres based on ZIF-8 and cellulose nanocrystal surface layers (ZIF-8/CNCs) were successfully prepared for the removal of malachite green. As a result of its porous structure, great specific surface area (1240 m^2 g^{-1}) and hydrophilic nature, the ZIF-8/CNC hybrid displayed a great adsorption ability of 1060.2 mg g^{-1} and re-usability for 3 cycles without loss of its structural properties and adsorption performance.[98] Li *et al.*[99] developed an *in situ* growth technique to successfully grow ZIF-8 on porous carbon (ZIF-8/porous carbon). This hybrid material was tested for the removal of MG from aqueous medium. The ZIF-8/porous carbon composite constructed at a carbon/Zn ratio of 1 : 4 demonstrated a superior adsorptive removal efficiency of malachite green (MG) with a reported maximum adsorption ability of 3056 mg g^{-1} at 30 °C. Furthermore, due to its high particle size, the 1 : 4 ZIF-8/porous carbon hybrid was readily separated through filtration and reused for 3 cycles with a retention of 88% of its original adsorption.[99] Abdi and co-authors[100] attempted to remove MG in an aqueous solution, and they studied the efficiency of two hybrids based on ZIF-8/GO and ZIF-8/carbon nanotubes (CNTs) towards the adsorption of MG. After the successful preparation of ZIF-8/CNT and ZIF-8/GO, new pores were observed for both hybrids, which were very useful for the adsorption of pollutant

molecules (MG). Furthermore, they showed that the construction of the ZIF-8/CNT and ZIF-8/GO hybrids prevented the generation of aggregates, achieving a high surface area of 830.3 $m^2\ g^{-1}$ and 1476.4 $m^2\ g^{-1}$, respectively. It was noted that the equilibrium data obtained were in very good accordance with the Langmuir model with MG adsorption capacities of 1667 mg g^{-1}, 3300 mg g^{-1} and 2034 mg g^{-1} for ZIF-8, ZIF-8/GO and ZIF-8/CNT, respectively. Moreover, the composites showed great recyclability for 4 cycles.[100] Nazir *et al.*[101] reported the development of a porous composite *via* the *in situ* growth of ZIF-8s on a layered double zinc hydroxide (ZnAl-LDH).

Compared to ZIF-8 alone, the ZIF-8/ZnAl-LDH hybrid displayed an improved adsorption capacity of 194.5 mg g^{-1}, and with a contact time of 180 min, a removal efficiency of 98% was recorded for MG dye. Moreover, the recyclability tests revealed that after 4 successive cycles, the ZIF-8/ZnAl-LDH composite exhibited an adsorption of 96.27% for MG compared to the initial capacity of the virgin ZIF-8/ZnAl-LDH.[101] Wang *et al.*[102] employed *in situ* polymerization to develop a novel composite aerogel based on egg yolk, ZIF-8 and cross-linked poly-acrylic acid (EY/ZIF-8/CLPAA). To improve the performance of the composite towards the removal of MG, they highlighted the effect of several parameters such as the effect of adsorbent dosage, which showed that when the dosage of the adsorbent increased, the amount of MG molecules adsorbed decreased, and the optimal dosage of the hybrid aerogel (EY/ZIF-8/CLPAA) was 2 mg, achieving an adsorption capacity of 2338 mg g^{-1}. Moreover, the Langmuir model was more applicable than the Freundlich model to describe the adsorption kinetics of MG because of its R^2 correlation coefficient, which was 1.00, while the R^2 correlation coefficient for the Freundlich model was 0.8916. These results confirmed that the adsorption process belonged to monolayer adsorption without interaction among the adsorbed molecules and without transport adsorption in between the adsorption sites.[102]

In addition to methylene blue, rhodamine B and malachite green, other pollutants have been removed using different ZIF-8-based composites, as listed in Table 1.

3. ZIF-8 materials for photocatalytic degradation of organic pollutants

Besides adsorption, other catalytic methods are commonly employed for treating water pollutants including primarily photocatalytic degradation, which represents "green technology" for removing harmful pollutants and other organic pollutants.[116–119] Compared to adsorption, photocatalytic processes can decompose organic pollutants such as MB, RhB, and MG into CO_2 and H_2O in the presence of a photocatalyst (ZIF-8). Thus far, ZIF-8 nanocrystals have been applied in the field of photocatalysis.[57,120–123] Nevertheless, due to their wide band gap (4.9–5.1 eV) and poor electron discharge capacity, their photocatalysis capabilities are generally lower than that of traditional semiconductors.[59] Consequently, several strategies have been developed to improve the efficiency of ZIF-8 for the removal of organic pollutants (MB, RhB, and MG) such as combining ZIF-8 with other semiconductors or doping ZIF-8 with elements to improve its optical properties and obtain

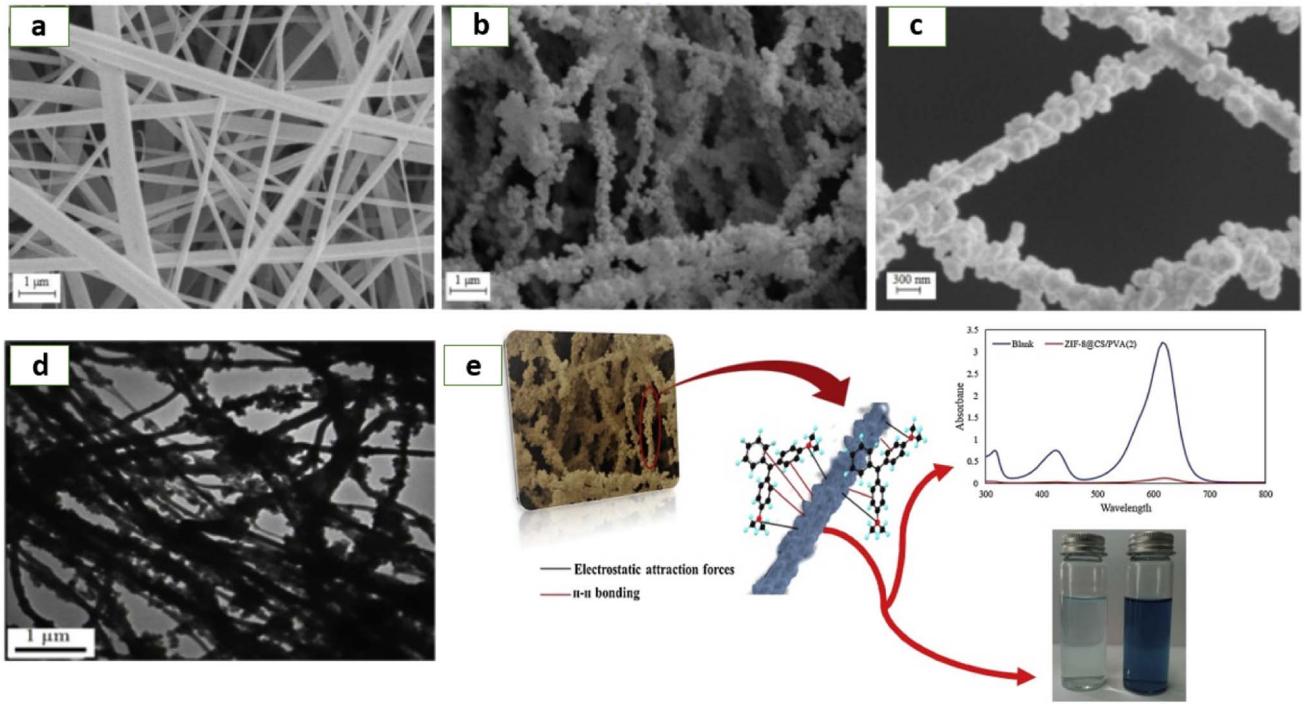

Fig. 5 SEM micrographs of engineered composites (a) CS/PVA-ENF and (b and c) ZIF-8-CS/PVA-ENF2. (d) TEM images of ZIF-8-CS/PVA-ENF2 hybrid. (e) Adsorption mechanism of malachite green on ZIF-8-CS/PVA-ENF2. Reproduced with permission from ref. 74 Copyright ©2020, Elsevier.

Table 1 A summary of the different ZIF-8 composites developed for the adsorption of various pollutants

Adsorbent	Synthesis method	S_{BET} ($m^2\ g^{-1}$)	Adsorption capacity ($mg\ g^{-1}$)	Pollutant	Ref.
ZIF-8/CS	*In situ* growth	—	922	CR	103
ZIF-8/Carbon fibers	*In situ* self-assembly method	97.32	42.64	CR	104
ZIF-8/$CoFe_2O_4$	Solid-phase extraction	918.9	52.04	CR	105
ZIF-8/ZnAl-LDH	*In situ* growth	963	609.7	MO	101
ZIF-8/SiO_2/$MnFe_2O$	Co-precipitation and modified Stöber method	830.3	78.12	MO	106
ZIF-8/graphene aerogels	Counter diffusion method	—	406.5	MO	93
EW/ZIF-8/PAA	*In situ* polymerization, freezing and freeze drying	—	297.1	MO	107
EY/ZIF-8/CLPAA	*In situ* polymerization	—	447	MO	102
ZIF8/Fe_3O_4/BNT	Solvothermal method	428.7	40.5	RO16	108
ACPMG/ZIF-8	Solvothermal method	1001.4	1250	SO	109
ZIF-8/SBA-15	LPE method	722	116.9	Bisphenol A	110
KGM/ZIF-8	Sol–gel and freeze-drying	—	812.35	Ciprofloxacin	111
ZIF-8/PAM	*In situ* method	14.4	111.5	Humic acid	112
ZIF-8/PDA/PAN	Self-polymerization	319.38	478.18	Tetracycline	50
Fe-doped ZIF-8	Precipitation method	1135	867	Tetracycline	92
ZIF-8/wool	*In situ* method	—	371.2–391.1	2-Naphthol	113
ZIF-8/GO	*In situ* method	946.5	171.3	1-Naphthylamine	114
ZIF-8/chitosan-g-PNVCL	Electrospinning method	—	152.3	Phenol	115

hybrids with improved photocatalytic performance. In this second part, we review the different ZIF-8-based photocatalysts been applied to degrade different organic pollutants such as MB, RhB, and MG.

3.1 Photocatalytic degradation of MB

Recently, Faraji *et al.*[124] exploited the magnetic properties of $NiFe_2O_4$ to form a ZIF-8/$NiFe_2O_4$-based composite, which could be easily separated from the reaction medium. The prepared photocatalyst was evaluated for the photocatalytic decomposition of methylene blue. They showed that the photocatalyst prepared with 30 wt% $NiFe_2O_4$ manifested the strongest photocatalytic behavior, resulting in a degradation efficacy of 94% within 120 min. This improvement was attributed to the addition of $NiFe_2O_4$, which extended the lifetime of the electron hole pairs. Moreover, its magnetic property allowed the composite to be regenerated and reused for 4 cycles without loss of its properties such as degradation efficiency (90%).[124] Chandra and co-authors[125] reported the synthesis of a composite named ZIF-8/AgNPs for the photocatalytic degradation of MB. Due to its large specific surface area (1370.91 $m^2\ g^{-1}$) and unique synergistic characteristics, the sample prepared with a 300 μL suspension of AgNPs displayed outstanding photocatalytic efficiency towards methylene blue with a degradation rate of 97% at pH ≥ 7. Furthermore, they demonstrated that upon the degradation of MB, the metallic AgNPs acted as electron collectors, which facilitated the transfer of photo-generated electrons into the conduction band (VB) of ZIF-8 as a result of surface plasmon resonance (SPR), and due to the synergistic effect of ZIF-8 and AgNPs, the pairs (e^-/h^+) readily reacted with water and oxygen to form species capable of mineralizing MB to CO_2 and H_2O.[125] Similarly, He *et al.*[57] reported the fabrication of a ZIF-8/AgBr composite photocatalyst *via* the solvothermal route, which was used for the photodecomposition of MB. The optical analysis showed that the coupling of ZIF-8 with AgBr resulted in improved light absorption efficiency; moreover, with a high content of AgBr, a red shift in the absorption edge was evident. The remarkable improvement in the charge separation efficiency was a result of the synergistic effect generated when coupling ZIF-8 with AgBr. The recorded MB decomposition rate was 0.0273 min^{-1}, which was 3.59-fold higher than that of AgBr. The stability and recyclability revealed that the photocatalyst with a weight of 40% AgBr (40% AgBr/ZIF-8) displayed very stable photocatalytic activity for 6 successive rounds.[57]

Guan *et al.*[126] synthesized an Ag/AgCl/ZIF-8/TiO_2/C-based composite on the surface of cotton fabric using a simple procedure. Under visible light irradiation, the Ag/AgCl/ZIF-8/TiO_2/C photocatalyst demonstrated a MB degradation efficiency of 98.5% within 105 min with a first-order kinetic constant of 0.0332 min^{-1}. Moreover, the photocatalytic decomposition capacity of methylene blue was 85% after 3 cycles, which implies the excellent stability of the Ag/AgCl/ZIF-8/TiO_2/C hybrid. In this work, they showed that ZIF-8 present in the developed composite acted as an oxygen molecule promoter during the photocatalytic decomposition process, where during this time, the photo-generated holes that existed in the valance band (VB) of the photocatalyst oxidized the water molecules into $OH^{\cdot}$, and therefore, hydroxyl radicals ($OH^{\cdot}$) and superoxides ($O_2^{\cdot -}$) were regarded as the radicals responsible for the photo-decomposition of MB. The mechanism of photo-degradation of MB is presented in Fig. 6a.[126] Another ternary system based on RGO/black TiO_2/2D-ZIF-8 was developed by He *et al.*,[127] which was used for the degradation of MB (Fig. 2b). The EIS analyses presented in Fig. 6c show that after the association of the 2D-ZIF-8 nanosheets, the RGO/black TiO_2/2D-ZIF-8 ternary hybrid displayed the lowest semicircle diameter, which means that RGO/BTiO_2/2D-ZIF-8 possessed the greatest charge carrier mobility. Moreover, they indicated that the insertion of 2D-ZIF-8 gave the ternary system a strong dye adsorption capacity and monitored the *in situ* decomposition at the adsorption site. It

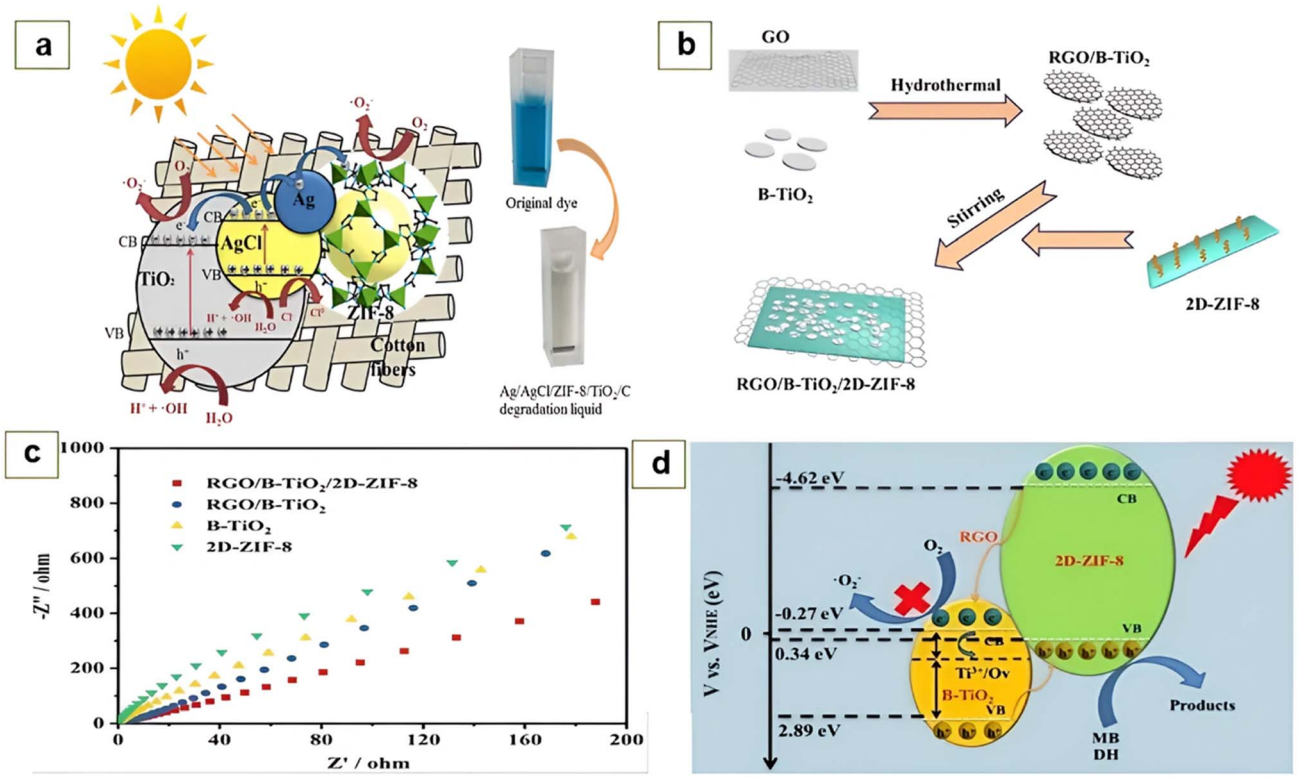

Fig. 6 (a) Photo-degradation mechanism of MB with Ag/AgCl/ZIF-8/TiO_2/C hybrid. Reproduced from ref. 126 Copyright 2019, Springer. (b) Process for the elaboration of the ternary system RGO/B TiO_2/2D-ZIF-8. (c) EIS analysis of B–TiO_2, RGO/B TiO_2, 2D-ZIF-8 and RGO/B TiO_2/2D-ZIF-8. (d) Photo-degradation mechanism of MB with RGO/B TiO_2/2D-ZIF-8 ternary system. Reproduced with permission from ref. 127 Copyright ©2020, Wiley VCH.

was found that the rate constant for the photocatalytic decomposition of methylene blue was 0.0232 min^{-1}, which was 3.3-times greater than that of black TiO_2. The photocatalytic decomposition mechanism of MB described in Fig. 6d shows that the photo-generated electrons at the surface of B TiO_2 cannot easily scavenge O_2 to generate $O_2^{\bullet -}$ given that the redox potential of the $O_2/O_2^{\bullet -}$ couple was more negative (−0.33 eV) than the conduction band energy of black TiO_2 (−0.27 eV). Moreover, it was well noted that the redox potential of the H_2O/OH^- couple (2.53 eV) was bigger than the valence band energy of ZIF-8 (0.34 eV), thus also rendering it infeasible for the photo-generated holes to generate $OH^{\bullet}$ radicals from H_2O. Consequently, the holes directly came in contact with MB during the photo-degradation pathway. Due to its great electrical conductivity, RGO also helped to effectively separate the electron/hole pairs, which decreased the recombination rate, and consequently improved the photo-degradation of MB.[127] Recently, Yurtsever and co-workers[128] investigated the influence of crystallization time and the quantity of zeolitic imidazolate framework-8 (ZIF-8) on the photocatalytic performance of ZIF-8-decorated copper-doped titania powders (Cu–TiO_2/ZIF-8). They demonstrated that with a decrease in the ZIF-8 content and growth time, the photocatalytic activity was enhanced, and the nanocomposites prepared at 5% ZIF-8 content and 15 min growth time displayed the highest photocatalytic activity with a 1st order rate constant 1.4- and 4-fold higher than that of pristine Cu–TiO_2 and ZIF-8, respectively. Alternatively, an additional increase in ZIF-8 level to 46% induced the clumping of these aggregates, leading to a reduction in photocatalytic activity.[128] Outstanding photocatalytic activity was obtained on cotton fabric (CF), which was treated with poly-dopamine (pDA), followed by the *in situ* deposition of ZIF-8/TiO_2 composites, leading to the formation of the ZIF-8/TiO_2/pDA/CF hybrid photocatalyst. The formed hybrid was evaluated for the photocatalytic decomposition of MB. The photoluminescence spectra revealed that the incorporation of ZIF-8 enhanced the charge transfer capability and lowered the percentage of pairs recombination (e^-/h^+), and the photo-degradation efficiency of MB obtained by this hybrid was 93.1% during 130 min of irradiation. This good activity was attributed to the great BET surface area of ZIF-8 and the self-polymerization of pDA, resulting in the formation of melanin, which could absorb the heat, and consequently accelerate the catalytic efficacy.[129] Employing an impregnation process, ZIF-8s decorated with carbon quantum dots (ZIF-8@CQDs) were developed and tested to remove methylene blue from the aqueous medium. A greater absorption ability and better response to visible light were obtained by the ZIF-8@CQD hybrid due to its core–shell structure, resulting in an MB removal efficiency of 91% and a 6-fold better rate constant than ZIF-8. Simultaneously, the ZIF-8@CQD photocatalyst was employed for three cycles of reuse, exhibiting outstanding structural stability without loss in its properties

such as catalytic activity.[130] Yang *et al.*[131] developed a novel photo-catalyst, where bismuth was doped in the ZIF-8/g-C_3N_4 heterojunction to form the Bi@g-C_3N_4/ZIF-8 composite. A decomposition efficiency of 86.6% within 60 min was obtained by the hybrid prepared with 12% of bismuth and a mass ratio of ZIF-8: g-C_3N_4 = 1.5 : 1. They explained that this efficiency was due to the effect of bismuth, which provided a suitable channel for photo-induced carrier transmission. Moreover, the synergistic effect of the inserted bismuth with the ZIF-8/g-C_3N_4 heterojunction also improved the light absorption performance, thermal stability and recyclability.[131] Due to its tight band gap and S–Mo–S sandwich coordination structure, MoS_2 was also considered as a semiconductor, which could further boost the catalytic performance of ZIF-8 by forming a ZIF-8/MoS_2-based hybrid.[132–134] As an example, Chen *et al.*[135] successfully assembled ZIF-8 on a carboxyl cotton cloth, and subsequently grew MoS_2 on the surface of ZIF-8 to form an MoS_2/ZIF-8/carboxyl cotton composite, which was capable of efficiently absorbing light and degrading MB. The fabric functionalized with 5 ZIF-8 layers (MZ-5/carboxyl-cotton) showed the best methylene blue degradability of about 99.8% for 21 min; moreover, a photocatalytic activity of about 94.8% was retained even 6 recycling cycles.

3.2 Photocatalytic degradation of RhB

Besides the photodegradation of methylene blue, other studies have been conducted to evaluate the potential of ZIF-8-based materials to mineralize rhodamine B (RhB). For example, Cao *et al.*[121] employed an *in situ* reaction to successfully coat manganese oxide (MnO_2) on a zeolitic framework of imidazolate-8 (ZIF-8). The formed ZIF-8@MnO_2 hybrid was used as a photocatalyst to decompose RhB in a Fenton-like procedure, yielding a decomposition rate of >96.0% for 120 min, whereas the degradation rate by the pristine ZIF-8s was 63%. These satisfactory results were attributed to the porous nature of ZIF-8s, which allowed the adsorption of more rhodamine B molecules; moreover, the anchoring of the MnO_2 nanoparticles (NPs) on ZIF-8 allowed their good dispersion to provide a larger active surface area. Consequently, the formation of the ZIF-8@MnO_2 heterojunction resulted in effective charge separation, which led to the high production of free radicals such as $OH^{\cdot}$. Yang *et al.*[136] developed a novel MOF-derived approach for the fabrication of ZIF-8/ZnO composite photocatalysts through the micro-catalysis process by employing ZIF-8 as the reagent and $AgNO_3$ as the catalyst. The adjustment of the $AgNO_3$ concentration showed that the sample prepared with 50 mM $AgNO_3$ solution (50 ZIF-8/ZnO) gave the highest degradation efficiency of about 98.17% compared to the other composites prepared with $AgNO_3$ (100 mM and 25 mM). Moreover, the ZIF-8/ZnO (50) hybrid exhibited strong photostability, translating to a photocatalytic efficiency of 95.54% after 4 cycles of reuse.[136] In another paper, Kong and co-authors[58] reported the fabrication of a core–shell heterostructure denoted as ZnO/CdS@ZIF8 for the photodegradation of RhB. They showed that spindle-shaped ZnO also delivered Zn^{2+} to form ZIF-8. Due to the great absorption capacity of ZIF-8s and their unique pore structure, the photocatalytic decomposition rate constant of RhB obtained by the ZnO/CdS@ZIF8 composite was 0.018 min^{-1}, while the rate constant obtained by the CdS/ZnO hybrid was 0.009 min^{-1}.[58] Zeng *et al.*[49] employed a sonochemical method and successfully designed a ZIF-8/TiO_2 heterojunction, which was intended for the photocatalytic degradation of rhodamine B. In comparison with the commercially available P25, ZIF-8/TiO_2 displayed a better degradation efficacy of rhodamine B. They showed that the encapsulation of ZIF-8 accelerated the photodegradation kinetics of RhB, where an N–Ti–O chemical bond was developed between TiO_2 and ZIF-8, which favored the efficient separation of electron/hole pairs. The O_2 molecules present in the reaction medium were trapped by the photogenerated e^- in the conduction band of the ZIF-8/TiO_2 composite to form $O_2^{\cdot -}$ superoxide radicals, which contributed to the mineralization of RhB.[49] In another study, Liu *et al.*[137] discussed the impact of the incorporation of ZIF-8 on the photocatalytic performance of Ag/AgCl. Firstly, the Ag/AgCl nanoparticles were encapsulated on the surface of ZIF-8 with a content of 50 wt%, resulting in the formation of an Ag/AgCl/ZIF-8 (50%) hybrid. The Ag/AgCl/ZIF-8-50% hybrid exhibited great absorption in the wavelength region of 420–800 nm as a result of the surface plasmon resonance (SPR) effect of the Ag particles formed *in situ* onto on surface of the AgCl NPs. Compared to Ag/AgCl, the Ag/AgCl/ZIF-8-50% composite showed outstanding photocatalytic activity, which was related to the dual active function of ZIF-8, *i.e.*, adsorption of rhodamine B and production of more $O_2^{\cdot -}$ superoxide radicals, which contributed to the mineralization of RhB.[137] Abdi *et al.*[138] successfully used a quick and easy method to fabricate a ZIF-8 photocatalyst doped with various Ag contents (ZIF-8@Ag-X). The photocatalyst was synthesized with 15% Ag content (ZIF-8@Ag-15%) showed the maximum RhB removal efficiency (93%) within 30 min of irradiation, and the rate constant recorded for this photocatalyst was 0.1016 min^{-1}. The inclusion of Ag nanoparticles on the surface of ZIF-8 substantially boosted the photodecomposition efficiency of RhB by scavenging the photogenerated electrons, thereby diminishing the possibility of charge recombination. The trapping investigations revealed that holes (h^+) and hydroxyl radicals ($OH^{\cdot}$) were the species responsible for the mineralization of RhB into CO_2 and H_2O.[138] Similarly, Jing *et al.*[139] employed a nucleating, precipitating, growing and photo-reducing approach to produce AgCl and Ag co-doped ZIF-8 photocatalysts. As a consequence of the synergistic effect among AgCl, Ag and ZIF-8, great visible light absorption ability was noticed by the hybrid made at an $AgNO_3$ concentration equal to 15 mM, showing a high rhodamine B degradation efficiency of 99.12% for 60 min of illumination, while that for Ag/AgCl was 94.24% and ZIF-8 (5.17%). Moreover, the photocatalytic efficacy of Ag/AgCl-15@ZIF-8 was reduced by only 1.96% after 4 repeated degradation rounds.[139] Chang *et al.*[140] constructed a Z-type heterojunction of AgCl/Ag-doped-ZIF-8. They reported the combination of AgCl with Ag-doped-ZIF-8 through a precipitation reaction, forming an AgCl/Ag-ZIF-8 heterojunction. It was noted that doping with Ag on ZIF-8s significantly lowered the gap energy, involving improved light harvesting. Moreover, the formation of the Z-

Table 2 Summary of the different ZIF-8 composites developed for the photodegradation of various pollutants

Photocatalyst	Synthesis method	Gap energy (eV)	Removal efficiency (%)	Pollutants	Ref.
ZIF-8@$CuInS_2$	Solvothermal process following by a reaction with methanol and PVP	1.96	90 87 74	Phenol Chlorophenol 2-Naphthalenesulfonic acid	142
ZIF-8/TiO_2	Hydrothermal method	2.98	90	Tetracycline	143
ZIF-8/g-C_3N_4	Exfoliating-wrapping	2.73	87.6	Tetracycline	144
ZIF-8/Cu_2O	*In situ* growth	4.31	84.1	Tetracycline	145
Ag-doped ZIF-8	Fast and facile process	3.2	93	Methyl orange	138
ZIF-8@AgNPS	*In situ* growth	5.13	100	Congo red	125
Ag/AgCl@ZIF-8/gC_3N_4	Simple process	—	94.5	Levofloxacin	146
ZIF-8/BiOI	Solvothermal process	1.55–1.88	82.5	Bisphenol A	147
Pt/TiO_2–ZnO@ZIF-8	Simple process	3.2	99.7	Phenol	148
ZIF-8/MoS_2	Solvothermal process	1.05	93.2 75.6	Ciprofloxacin Tetracycline hydrochloride	149
ZIF-8/CdS	ZIF-8 crystal self-assembled around PVP-embedded CdSNPs	2.05	81.69	Toluene	150
ZIF-8/Fe_2O_3	Green method	—	94	Reactive Red 198	151

type heterojunction of AgCl/Ag-doped-ZIF-8 also contributed to the improvement in the catalytic performance of the photocatalyst, given that it enabled the effective separation of the photo-generated charges. The photocatalytic activity achieved by the AgCl/Ag-ZIF-8 heterojunction was found to be 12-fold better that the virgin ZIF-8, with high stability and reusability.[140] Similarly, He and co-authors[57] used a ZIF-8/AgBr hybrid for the photodegradation of RhB. The optical analysis showed that the coupling of ZIF-8 with AgBr resulted in improved light absorption efficiency, and the photodecomposition rate of RhB recorded by the ZIF-8/AgBr hybrid was 98.5% during 60 min irradiation and the rate constant was about 0.115 min^{-1}[57].

3.3 Photocatalytic degradation malachite green

Recently, Abdollahi *et al.*[123] employed a precipitation process to grow a CuO–ZnO/ZiF-8 hybrid photocatalyst. The developed composite was evaluated for the photocatalytic degradation of malachite green. They observed using DRS analysis that the sample developed with a ZIF-8 content equal to 20 wt% (CuO–ZnO/ZiF-8-20) demonstrated a tighter gap energy (1.96 eV) than of ZIF-8 (5.34 eV) and CuO–ZnO (2.89 eV). Also, the inclusion of ZIF-8 on the CuO–ZnO heterojunction resulted in an increase in specific surface area from 12.3 $m^2 g^{-1}$ (CuO–ZnO) to 22.2 $m^2 g^{-1}$ (CuO–ZnO/ZiF-8-20). As a result of this increase, the photocatalyst adsorbed a large quantity of the dye, which was subsequently degraded by visible light. The photocatalytic activity recorded by the CuO–ZnO/ZiF-8-20 photocatalyst towards the removal of MG with a concentration of 80 ppm at pH 7 was 51%.[123] Alternatively, Li *et al.*[141] developed an approach based on the conversion of MIL-68(In)@ZIF-8 organometallic frameworks into an In_2O_3@ZnO heterostructure. They reported that the conversion was performed according to the calcination of MIL-68(In)@ZIF-8 to form core–shell hollow-microtubes of In_2O_3@ZnO intended for photodegradation of MG. The synthesized heterostructure showed an enhanced photocatalytic efficiency for the decomposition of MG compared to MIL-68(In)-derived In_2O_3 and ZIF-8-derived ZnO under light irradiation. Moreover, the In_2O_3@ZnO hybrid formed from MIL-68(In)@ZIF-8 provided a higher BET surface area, exposed more active sites, possessed a suitable amount of oxygen vacancies, better light absorption and efficiently stimulated photo-induced charge carrier transfer and separation. The photocatalytic activity registered by this heterostructure was 80.6% during 200 min of irradiation.[141]

In addition to methylene blue, rhodamine B and malachite green, other pollutants have been removed by different ZIF-8-based composites, as listed in Table 2.

4. Conclusion and prospects

In this review, we discussed the use of the ZIF-8 metal organic framework for the fabrication of composite materials for the removal and photocatalytic degradation of organic pollutants. The adsorption and photocatalysis of persistent organic contaminants are viable and economically feasible methods. Accordingly, the development of stable, selective and robust adsorbents is a promising route to achieve a sustainable future. Particularly, MOFs and ZIF-8 are high-surface area materials, playing a vital role for surface retention of organic pollutants. Improving the pore size and structure of ZIF-8 through metal doping, formation of composites and functionalization is considered necessary to enhance to adsorption capacity due to synergistic effect of ZIF-8 and the doped and composite materials. Additionally, morphological, optical and chemical properties tunability can be an asset for enhancing the photocatalytic degradation efficiency. Chemists and physicists

devoting tremendous efforts to the synthesis and application of photo-active ZIF-8 materials for environmental remediation.

However, although there have been remarkable achievements in the last decade in this regard for the removal and photocatalytic degradation of organic pollutants, it is still far from real practical application. Thus, herein, we propose the following points for future development:

4.1. Scalability and stability

Pilot-scale synthesis of ZIF-8-based composites with high yields using flow reactors should be considered and stable materials in real world applications should be envisaged.

4.2. Cost

Reducing the cost for the synthesis of ZIF-8 materials with a targeted surface area, optical absorption and crystallinity. This includes low energy consumption in synthesis strategies (temperature, pressure) and low-cost reagents to avoid the use of organic solvents.

4.3. Real application

Real wastewater experiments in continuous flow reactors (water treatment plants) should be evaluated. Wastewater usually has dye concentrations of 200 ppm, while the lab-scale experiments in adsorption and photocatalysis deal only with concentrations of dyes as low as 50 ppm.

4.4. New insights

Exploring the mechanistic fundamental study to assess the stability of adsorbents/photocatalysts and the identification reaction intermediates. DFT calculations can be performed to elaborate a full concise comprehensive study.

4.5. Sustainability

The mineralization should be studied and reported. The toxicity of intermediates during the reaction process and the leachability of ZIF-8 adsorbent/photocatalysts should be studied to guarantee the environmental friendliness and sustainability of the materials.

Author contributions

Aicha Elaouni: writing the draft, data curation; formal analysis. Mohamed El ouardi: writing the draft, data curation; formal analysis. Mohamed Zbair: writing – review & editing; project administration. Hassan Ait Ahsaine: writing the draft, project administration; supervision and validation. Amal BaQais: writing – review & editing; project administration. Mohamed Saadi: project administration; supervision and validation.

Conflicts of interest

The author declares that he has no known competing financial interests or personal relationships that could have appeared to influence the work reported in this paper.

Acknowledgements

We thank all the authors and their respective institutions.

References

1 M. M. S. Abbassy, *Mar. Pollut. Bull.*, 2018, **131**, 115–121.
2 P. Xiong, H. Zhang, G. Li, C. Liao and G. Jiang, *Sci. Total Environ.*, 2021, **797**, 149179.
3 J. O. Ighalo, S. Rangabhashiyam, C. A. Adeyanju, S. Ogunniyi, A. G. Adeniyi and C. A. Igwegbe, *J. Ind. Eng. Chem.*, 2022, **105**, 34–48.
4 Md. M. H. Mondol and S. H. Jhung, *Chem. Eng. J.*, 2021, **421**, 129688.
5 J. Gasperi, C. Sebastian, V. Ruban, M. Delamain, S. Percot, L. Wiest, C. Mirande, E. Caupos, D. Demare, M. D. K. Kessoo, M. Saad, J. J. Schwartz, P. Dubois, C. Fratta, H. Wolff, R. Moilleron, G. Chebbo, C. Cren, M. Millet, S. Barraud and M. C. Gromaire, *Environ. Sci. Pollut. Res.*, 2014, **21**, 5267–5281.
6 J. O. Ighalo, O. J. Ajala, G. Umenweke, S. Ogunniyi, C. A. Adeyanju, C. A. Igwegbe and A. G. Adeniyi, *J. Environ. Chem. Eng.*, 2020, **8**, 104264.
7 K. Kemp, J. Griffiths, S. Campbell and K. Lovell, *Journal of Crohn's and Colitis*, 2013, **7**, e386–e395.
8 M. F. Abid, M. A. Zablouk and A. M. Abid-Alameer, *Iran. J. Environ. Health Sci. Eng.*, 2012, **9**, 1–9.
9 J. Jawad, A. H. Hawari and S. J. Zaidi, *Chem. Eng. J.*, 2021, 129540.
10 X. Wang, J. Xu, M. Xu, B. Zhou, J. Liang and L. Zhou, *Sep. Purif. Technol.*, 2021, **258**, 118047.
11 A. Chennah, Y. Naciri, H. A. Ahsaine, A. Taoufyq, B. Bakiz, L. Bazzi, F. Guinneton, J.-R. Gavarri and A. Benlhachemi, *Mediterr. J. Chem.*, 2018, **6**, 255–266.
12 H. A. Ahsaine, A. Slassi, Y. Naciri, A. Chennah, C. Jaramillo-Páez, Z. Anfar, M. Zbair, A. Benlhachemi and J. A. Navío, *ChemistrySelect*, 2018, **3**, 7778–7791.
13 H. Ait Ahsaine, M. Ezahri, A. Benlhachemi, B. Bakiz, S. Villain, F. Guinneton and J.-R. Gavarri, *Ceram. Int.*, 2016, **42**, 8552–8558.
14 Y. Naciri, H. Ait Ahsaine, A. Chennah, A. Amedlous, A. Taoufyq, B. Bakiz, M. Ezahri, S. Villain and A. Benlhachemi, *J. Environ. Chem. Eng.*, 2018, **6**, 1840–1847.
15 M. El Ouardi, A. El aouni, H. A. Ahsaine, M. Zbair, A. BaQais and M. Saadi, *Chemosphere*, 2022, 136483.
16 S. Lotfi, M. E. Ouardi, H. A. Ahsaine and A. Assani, *Catal. Rev.*, 2022, 1–45.
17 A. Bouddouch, E. Amaterz, B. Bakiz, A. Taoufyq, F. Guinneton, S. Villain, J.-R. Gavarri, J.-C. Valmalette and A. Benlhachemi, *Minerals*, 2021, **11**, 1007.
18 R. Haounati, F. Alakhras, H. Ouachtak, T. A. Saleh, G. Al-Mazaideh, E. Alhajri, A. Jada, N. Hafid and A. A. Addi, *Arabian J. Sci. Eng.*, 2022, 1–11.
19 K. Aziz, F. Aziz, R. Mamouni, L. Aziz, Z. Anfar, A. Azrrar, B. Kjidaa, N. Saffaj and A. Laknifli, *Environ. Sci. Pollut. Res.*, 2021, DOI: **10.1007/s11356-021-16340-w**.

20 R. Haounati, A. El Guerdaoui, H. Ouachtak, R. El Haouti, A. Bouddouch, N. Hafid, B. Bakiz, D. M. F. Santos, M. Labd Taha, A. Jada and A. Ait Addi, *Sep. Purif. Technol.*, 2021, **277**, 119399.
21 K. Y. V. Beri, D. P. Barbosa, M. Zbair, S. Ojala and S. B. de Oliveira, *Energy Nexus*, 2021, **1**, 100009.
22 C. Du, Z. Zhang, G. Yu, H. Wu, H. Chen, L. Zhou, Y. Zhang, Y. Su, S. Tan, L. Yang, J. Song and S. Wang, *Chemosphere*, 2021, **272**, 129501.
23 J. Wen, Y. Fang and G. Zeng, *Chemosphere*, 2018, **201**, 627–643.
24 J. Huang, D. Huang, F. Zeng, L. Ma and Z. Wang, *J. Mater. Sci.*, 2021, **56**, 3127–3139.
25 R. Wang, H. Xu, K. Zhang, S. Wei and W. Deyong, *J. Hazard. Mater.*, 2019, **364**, 272–280.
26 V. K. Sharma and M. Feng, *J. Hazard. Mater.*, 2019, **372**, 3–16.
27 B. Chen, Z. Yang, Y. Zhu and Y. Xia, *J. Mater. Chem. A*, 2014, **2**, 16811–16831.
28 B. Liu, M. Jian, H. Wang, G. Zhang, R. Liu, X. Zhang and J. Qu, *Colloids Surf., A*, 2018, **538**, 164–172.
29 V. Anh Tran, L. T. Nhu Quynh, T.-T. Thi Vo, P. A. Nguyen, T. N. Don, Y. Vasseghian, H. Phan and S.-W. Lee, *Environ. Res.*, 2022, **204**, 112364.
30 Z. Tang, F. Zhu, J. Zhou, W. Chen, K. Wang, M. Liu, N. Wang and N. Li, *Appl. Catal., B*, 2022, **309**, 121267.
31 J. Liu, Y. Chen, Y. Hu, Y. Zhang, G. Zhang, S. Wang and L. Zhang, *J. Mol. Liq.*, 2022, **356**, 119057.
32 J. Troyano, A. Carné-Sánchez, C. Avci, I. Imaz and D. Maspoch, *Chem. Soc. Rev.*, 2019, **48**, 5534–5546.
33 R. Banerjee, A. Phan, B. Wang, C. Knobler, H. Furukawa, M. O'Keeffe and O. M. Yaghi, *Science*, 2008, **319**, 939–943.
34 J. Lee, K. Lee and J. Kim, *ACS Appl. Mater. Interfaces*, 2021, **13**, 1620–1631.
35 Q. Jiang, Z. Han, Y. Qian, Y. Yuan, Y. Ren, M. Wang and Z. Cheng, *Journal of Water Process Engineering*, 2022, **47**, 102768.
36 A. I. A. Soliman, A.-M. A. Abdel-Wahab and H. Nasser Abdelhamid, *RSC Adv.*, 2022, **12**, 7075–7084.
37 H. Bux, F. Liang, Y. Li, J. Cravillon, M. Wiebcke and J. Caro, *J. Am. Chem. Soc.*, 2009, **131**, 16000–16001.
38 K. W. Chapman, G. J. Halder and P. J. Chupas, *J. Am. Chem. Soc.*, 2009, **131**, 17546–17547.
39 V. V. Butova, A. P. Budnyk, E. A. Bulanova, C. Lamberti and A. V. Soldatov, *Solid State Sci.*, 2017, **69**, 13–21.
40 E. R. Cooper, C. D. Andrews, P. S. Wheatley, P. B. Webb, P. Wormald and R. E. Morris, *Nature*, 2004, **430**, 1012–1016.
41 W. Lin, J. Gong, W. Ye, X. Huang and J. Chen, *Z. Anorg. Allg. Chem.*, 2020, **646**, 1900–1903.
42 H. Zheng, D. Wu, Y. Wang, X. Liu, P. Gao, W. Liu, J. Wen and E. V. Rebrov, *J. Alloys Compd.*, 2020, **838**, 155219.
43 M. P. M. Dicker, P. F. Duckworth, A. B. Baker, G. Francois, M. K. Hazzard and P. M. Weaver, *Composites, Part A*, 2014, **56**, 280–289.
44 G. Lu, S. Li, Z. Guo, O. K. Farha, B. G. Hauser, X. Qi, Y. Wang, X. Wang, S. Han, X. Liu, J. S. DuChene, H. Zhang, Q. Zhang, X. Chen, J. Ma, S. C. J. Loo, W. D. Wei, Y. Yang, J. T. Hupp and F. Huo, *Nat. Chem.*, 2012, **4**, 310–316.
45 T. Li, W. Zhang, S. Zhai, G. Gao, J. Ding, W. Zhang, Y. Liu, X. Zhao, B. Pan and L. Lv, *Water Res.*, 2018, **143**, 87–98.
46 Q.-L. Zhu and Q. Xu, *Chem. Soc. Rev.*, 2014, **43**, 5468–5512.
47 B. Yu, F. Wang, W. Dong, J. Hou, P. Lu and J. Gong, *Mater. Lett.*, 2015, **156**, 50–53.
48 X. Wang, J. Liu, S. Leong, X. Lin, J. Wei, B. Kong, Y. Xu, Z.-X. Low, J. Yao and H. Wang, *ACS Appl. Mater. Interfaces*, 2016, **8**, 9080–9087.
49 X. Zeng, L. Huang, C. Wang, J. Wang, J. Li and X. Luo, *ACS Appl. Mater. Interfaces*, 2016, **8**, 20274–20282.
50 S. Chao, X. Li, Y. Li, Y. Wang and C. Wang, *J. Colloid Interface Sci.*, 2019, **552**, 506–516.
51 Y. Zhang and S.-J. Park, *Appl. Catal., B*, 2019, **240**, 92–101.
52 H. Zheng, Z. Yang, W. Wang, S. Guo, Z. Li, K. Liu and N. Sui, *Plant Physiol. Biochem.*, 2020, **149**, 11–26.
53 P. Zhang, S. Wang, B. Y. Guan and X. W. David Lou, *Energy Environ. Sci.*, 2019, **12**, 164–168.
54 M. Hu, H. Lou, X. Yan, X. Hu, R. Feng and M. Zhou, *Microporous Mesoporous Mater.*, 2018, **271**, 68–72.
55 I. Ahmed, B. N. Bhadra, H. J. Lee and S. H. Jhung, *Catal. Today*, 2018, **301**, 90–97.
56 Q. T. N. Le and K. Cho, *J. Colloid Interface Sci.*, 2021, **581**, 741–750.
57 Y. He, L. Zeng, Z. Feng, Q. Zhang, X. Zhao, S. Ge, X. Hu and H. Lin, *Adv. Powder Technol.*, 2020, **31**, 439–447.
58 R.-M. Kong, Y. Zhao, Y. Zheng and F. Qu, *RSC Adv.*, 2017, **7**, 31365–31371.
59 H. Dai, X. Yuan, L. Jiang, H. Wang, J. Zhang, J. Zhang and T. Xiong, *Coord. Chem. Rev.*, 2021, **441**, 213985.
60 N. Ouasfi, S. Bouzekri, M. Zbair, H. Ait Ahsaine, S. Bakkas, M. Bensitel and L. Khamliche, *Surf. Interfaces*, 2019, **14**, 61–71.
61 H. Ait Ahsaine, M. Zbair, Z. Anfar, Y. Naciri, R. El haouti, N. El Alem and M. Ezahri, *Mater. Today Chem.*, 2018, **8**, 121–132.
62 M. Zbair, Z. Anfar and H. A. Ahsaine, *RSC Adv.*, 2019, **9**, 5756–5769.
63 Z. Anfar, H. Ait Ahsaine, M. Zbair, A. Amedlous, A. Ait El Fakir, A. Jada and N. El Alem, *Crit. Rev. Environ. Sci. Technol.*, 2020, **50**, 1043–1084.
64 Z. Anfar, M. Zbair, H. A. Ahsaine, A. Jada and N. E. Alem, *RSC Adv.*, 2020, **10**, 13430.
65 D. Allouss, Y. Essamlali, O. Amadine, A. Chakir and M. Zahouily, *RSC Adv.*, 2019, **9**, 37858–37869.
66 M. Zbair, M. Bottlinger, K. Ainassaari, S. Ojala, O. Stein, R. L. Keiski, M. Bensitel and R. Brahmi, *Waste Biomass Valorization*, 2020, **11**, 1565–1584.
67 M. Zbair, A. El Hadrami, A. Bellarbi, M. Monkade, A. Zradba and R. Brahmi, *J. Environ. Chem. Eng.*, 2020, **8**, 103667.
68 X. Zhao, M. Zheng, X. Gao, J. Zhang, E. Wang and Z. Gao, *Coord. Chem. Rev.*, 2021, **440**, 213970.
69 I. Cota and F. Fernandez Martinez, *Coord. Chem. Rev.*, 2017, **351**, 189–204.
70 Z. Chang, L. Zeng, C. Sun, P. Zhao, J. Wang, L. Zhang, Y. Zhu and X. Qi, *Coord. Chem. Rev.*, 2021, **445**, 214072.

71 D. Yamamoto, T. Maki, S. Watanabe, H. Tanaka, M. T. Miyahara and K. Mae, *Chem. Eng. J.*, 2013, **227**, 145–150.
72 Q. Zhu, W. Zhuang, Y. Chen, Z. Wang, B. Villacorta Hernandez, J. Wu, P. Yang, D. Liu, C. Zhu, H. Ying and Z. Zhu, *ACS Appl. Mater. Interfaces*, 2018, **10**, 16066–16076.
73 L. Zhao, W. Lv, J. Hou, Y. Li, J. Duan and S. Ai, *Microchem. J.*, 2020, **152**, 104425.
74 N. M. Mahmoodi, M. Oveisi, A. Taghizadeh and M. Taghizadeh, *Carbohydr. Polym.*, 2020, **227**, 115364.
75 W. Dong, D. Wang, H. Wang, M. Li, F. Chen, F. Jia, Q. Yang, X. Li, X. Yuan, J. Gong, H. Li and J. Ye, *J. Colloid Interface Sci.*, 2019, **535**, 444–457.
76 J. L. C. Rowsell and O. M. Yaghi, *J. Am. Chem. Soc.*, 2006, **128**, 1304–1315.
77 J. Zheng, C. Cheng, W.-J. Fang, C. Chen, R.-W. Yan, H.-X. Huai and C.-C. Wang, *CrystEngComm*, 2014, **16**, 3960–3964.
78 X. Wu, J. Xiong, S. Liu, J.-H. Cheng, M.-H. Zong and W.-Y. Lou, *J. Hazard. Mater.*, 2021, **417**, 126011.
79 Y. Zhan, X. Guan, E. Ren, S. Lin and J. Lan, *J. Polym. Res.*, 2019, **26**, 145.
80 N. Marsiezade and V. Javanbakht, *Int. J. Biol. Macromol.*, 2020, **162**, 1140–1152.
81 H. Nasser Abdelhamid and A. P. Mathew, *Chem. Eng. J.*, 2021, **426**, 131733.
82 L. Zhu, L. Zong, X. Wu, M. Li, H. Wang, J. You and C. Li, *ACS Nano*, 2018, **12**, 4462–4468.
83 W. Zhang, S. Shi, W. Zhu, L. Huang, C. Yang, S. Li, X. Liu, R. Wang, N. Hu, Y. Suo, Z. Li and J. Wang, *ACS Sustainable Chem. Eng.*, 2017, **5**, 9347–9354.
84 L. Zong, Y. Yang, H. Yang and X. Wu, *ACS Appl. Mater. Interfaces*, 2020, **12**, 7295–7301.
85 Y. Li, P. Kamdem and X.-J. Jin, *J. Electrochem. Soc.*, 2020, **167**, 110562.
86 C. Gu, W. Weng, C. Lu, P. Tan, Y. Jiang, Q. Zhang, X. Liu and L. Sun, *Chin. J. Chem. Eng.*, 2022, **42**, 42–48.
87 R. Li, X. Ren, J. Zhao, X. Feng, X. Jiang, X. Fan, Z. Lin, X. Li, C. Hu and B. Wang, *J. Mater. Chem. A*, 2014, **2**, 2168–2173.
88 X. Meng, C. Duan, Y. Zhang, W. Lu, W. Wang and Y. Ni, *Compos. Sci. Technol.*, 2020, **200**, 108384.
89 C. Fan, Y. Liang, H. Dong, J. Yang, G. Tang, W. Zhang, D. Kong, J. Li and Y. Cao, *Sci. Total Environ.*, 2018, **640–641**, 163–173.
90 X. Chen, Y. Zhang, Y. Zhao, Y. Wu, S. Wang, W. Xu, J. Zhang, S. Yang, L. Liu and Y. Liu, *Mater. Lett.*, 2018, **218**, 67–70.
91 L. Yin, Z. Liu, Y. Yang, Y. Guo, G. Zhang, F. Gai, Y. Ao, jieran Liu, B. Xin and Y. Liu, *Mater. Chem. Phys.*, 2020, **242**, 122563.
92 H. Yang, S. Hu, H. Zhao, X. Luo, Y. Liu, C. Deng, Y. Yu, T. Hu, S. Shan, Y. Zhi, H. Su and L. Jiang, *J. Hazard. Mater.*, 2021, **416**, 126046.
93 P. Hou, G. Xing, D. Han, H. Wang, C. Yu and Y. Li, *J. Solid State Chem.*, 2018, **265**, 184–192.
94 M. Hijab, P. Parthasarathy, H. R. Mackey, T. Al-Ansari and G. McKay, *Chem. Eng. Process.*, 2021, **167**, 108318.
95 X. Fan, L. Deng, K. Li, H. Lu, R. Wang and W. Li, *Colloid Interface Sci. Commun.*, 2021, **44**, 100485.
96 B. Yan, X. Wang, X. Zhang, S. Liu, H. Lu and R. Ran, *Colloids Surf., A*, 2022, **639**, 128347.
97 S. B. Zadvarzi, M. Khavarpour, S. M. Vahdat, S. M. Baghbanian and A. S. Rad, *Int. J. Biol. Macromol.*, 2021, **168**, 428–441.
98 J. Ma, J. Hu, Y. Tang, H. Gu, M. Jiang and J. Zhang, *J. Colloid Interface Sci.*, 2020, **572**, 160–169.
99 Y. Li, X. Yan, X. Hu, R. Feng, M. Zhou and D. Han, *J. Porous Mater.*, 2020, **27**, 1109–1117.
100 J. Abdi, M. Vossoughi, N. M. Mahmoodi and I. Alemzadeh, *Chem. Eng. J.*, 2017, **326**, 1145–1158.
101 M. A. Nazir, M. A. Bashir, T. Najam, M. S. Javed, S. Suleman, S. Hussain, O. P. Kumar, S. S. A. Shah and A. ur Rehman, *Microchem. J.*, 2021, **164**, 105973.
102 Q. Wang, X. Zhang, F. Wang, Y. Xie, C. Wang, J. Zhao, Q. Yang and Z. Chen, *J. Solid State Chem.*, 2021, **299**, 122158.
103 Y. Wang, X. Dai, Y. Zhan, X. Ding, M. Wang and X. Wang, *Int. J. Biol. Macromol.*, 2019, **137**, 77–86.
104 S.-Q. Xiong, J.-L. Li, Y. Wang, Y.-H. Gao, C.-X. Jin, W.-W. Dong, J. Zhao, M. He, D. Li and H.-B. Shang, *ChemistrySelect*, 2019, **4**, 6429–6436.
105 Y. Xu, J. Jin, X. Li, Y. Han, H. Meng, J. Wu and X. Zhang, *J. Sep. Sci.*, 2016, **39**, 3647–3654.
106 J. Abdi, N. M. Mahmoodi, M. Vossoughi and I. Alemzadeh, *Microporous Mesoporous Mater.*, 2019, **273**, 177–188.
107 Q. Wang, L. Lei, F. Wang, C. Chen, X. Kang, C. Wang, J. Zhao, Q. Yang and Z. Chen, *J. Solid State Chem.*, 2020, **292**, 121656.
108 Ü. Ecer, A. Zengin and T. Şahan, *Colloids Surf., A*, 2021, **630**, 127558.
109 S. Sharafinia, A. Farrokhnia and E. G. Lemraski, *Colloids Surf., A*, 2022, **634**, 128039.
110 J. Peng, Y. Li, X. Sun, C. Huang, J. Jin, J. Wang and J. Chen, *ACS Appl. Mater. Interfaces*, 2019, **11**, 4328–4337.
111 Y. Yuan, D. Yang, G. Mei, X. Hong, J. Wu, J. Zheng, J. Pang and Z. Yan, *Colloids Surf., A*, 2018, **544**, 187–195.
112 O. Maan, P. Song, N. Chen and Q. Lu, *Adv. Mater. Interfaces*, 2019, **6**, 1801895.
113 R. M. Abdelhameed and H. E. Emam, *J. Colloid Interface Sci.*, 2019, **552**, 494–505.
114 J. Wang, Y. Li, Z. Lv, Y. Xie, J. Shu, A. Alsaedi, T. Hayat and C. Chen, *J. Colloid Interface Sci.*, 2019, **542**, 410–420.
115 E. Bahmani, S. Koushkbaghi, M. Darabi, A. ZabihiSahebi, A. Askari and M. Irani, *Carbohydr. Polym.*, 2019, **224**, 115148.
116 B. Akhsassi, A. Bouddouch, Y. Naciri, B. Bakiz, A. Taoufyq, C. Favotto, S. Villain, F. Guinneton and A. Benlhachemi, *Chem. Phys. Lett.*, 2021, **783**, 139046.
117 H. A. Ahsaine, A. E. Jaouhari, A. Slassi, M. Ezahri, A. Benlhachemi, B. Bakiz, F. Guinneton and J.-R. Gavarri, *RSC Adv.*, 2016, **6**, 101105–101114.
118 H. Ait Ahsaine, *Mater. Lett.*, 2020, **276**, 128221.

119 A. Bouddouch, E. Amaterz, A. Taoufyq, B. Bakiz, F. Guinneton, S. Villain, J. C. Valmalette, J. R. Gavarri and A. Benlhachemi, *Mater. Today: Proc.*, 2020, **27**, 3139–3144.
120 E. Shamsaei, F. Basquiroto de Souza, K. Sagoe-Crentsil and W. Duan, *Microporous Mesoporous Mater.*, 2022, **332**, 111702.
121 M. Cao, Z. Zhuang, Y. Liu, Z. Zhang, J. Xuan, Q. Zhang and W. Wang, *J. Colloid Interface Sci.*, 2022, **608**, 2779–2790.
122 H.-P. Jing, C.-C. Wang, Y.-W. Zhang, P. Wang and R. Li, *RSC Adv.*, 2014, **4**, 54454–54462.
123 B. Abdollahi, A. Najafidoust, E. Abbasi Asl and M. Sillanpaa, *Arabian J. Chem.*, 2021, **14**, 103444.
124 A. Faraji, N. Mehrdadi, N. M. Mahmoodi, M. Baghdadi and A. Pardakhti, *J. Mol. Struct.*, 2021, **1223**, 129028.
125 R. Chandra and M. Nath, *Journal of Water Process Engineering*, 2020, **36**, 101266.
126 X. Guan, S. Lin, J. Lan, J. Shang, W. Li, Y. Zhan, H. Xiao and Q. Song, *Cellulose*, 2019, **26**, 7437–7450.
127 J. He, J. Ye, Y. Zhang, L. Kong, X. Zhou, Y. Ma and Y. Yang, *ChemistrySelect*, 2020, **5**, 3746–3755.
128 H. A. Yurtsever and A. E. Çetin, *Colloids Surf., A*, 2021, **625**, 126980.
129 J. Ran, H. Chen, S. Bi, Q. Guo, C. Yan, X. Tang, D. Cheng, G. Cai and X. Wang, *Prog. Org. Coat.*, 2021, **152**, 106123.
130 Y. Si, X. Li, G. Yang, X. Mie and L. Ge, *J. Mater. Sci.*, 2020, **55**, 13049–13061.
131 Q. Yang, W. Lin, Z. Duan, S. Xu, J. Chen and X. Mai, *Environ. Technol.*, 2021, 1–13.
132 L. Lei, D. Huang, G. Zeng, M. Cheng, D. Jiang, C. Zhou, S. Chen and W. Wang, *Coord. Chem. Rev.*, 2019, **399**, 213020.
133 S. Zhang, C. Liu, G. Zhang, Y. Chen, F. Shang, Q. Xia and W. Yang, *Coord. Chem. Rev.*, 2021, **433**, 213742.
134 A. A. Ansari and B. D. Malhotra, *Coord. Chem. Rev.*, 2022, **452**, 214282.
135 H. Chen, Y.-Q. wang, F. Huang, C. Tu and li Cui, *Appl. Surf. Sci.*, 2021, **565**, 150458.
136 X. Yang, Z. Wen, Z. Wu and X. Luo, *Inorg. Chem. Front.*, 2018, **5**, 687–693.
137 J. Liu, R. Li, Y. Wang, Y. Wang, X. Zhang and C. Fan, *J. Alloys Compd.*, 2017, **693**, 543–549.
138 J. Abdi, *Colloids Surf., A*, 2020, **604**, 125330.
139 Y. Jing, Q. Lei, C. Xia, Y. Guan, Y. Yang, J. He, Y. Yang, Y. Zhang and M. Yan, *RSC Adv.*, 2020, **10**, 698–704.
140 N. Chang, Y.-R. Chen, F. Xie, Y.-P. Liu and H.-T. Wang, *Colloids Surf., A*, 2021, **616**, 126351.
141 J. Li, L. Liu, Q. Liang, M. Zhou, C. Yao, S. Xu and Z. Li, *J. Hazard. Mater.*, 2021, **414**, 125395.
142 A. Liu, C. Yu, J. Lin, G. Sun, G. Xu, Y. Huang, Z. Liu and C. Tang, *Mater. Res. Bull.*, 2019, **112**, 147–153.
143 R. Li, W. Li, C. Jin, Q. He and Y. Wang, *J. Alloys Compd.*, 2020, **825**, 154008.
144 X. Yuan, S. Qu, X. Huang, X. Xue, C. Yuan, S. Wang, L. Wei and P. Cai, *Chem. Eng. J.*, 2021, **416**, 129148.
145 Y. Zhou, S. Feng, X. Duan, W. Wu, Z. Ye, X. Dai, Y. Wang and X. Cao, *J. Solid State Chem.*, 2022, **305**, 122628.
146 J. Zhou, W. Liu and W. Cai, *Sci. Total Environ.*, 2019, **696**, 133962.
147 W. Zheng, S. Feng, C. Shao, G. Zhu, Z. Ni, J. Sun and X. Huang, *Res. Chem. Intermed.*, 2020, **46**, 2951–2967.
148 Y. Jing, H. Yin, C. Li, J. Chen, S. Wu, H. Liu, L. Xie, Q. Lei, M. Sun and S. Yu, *Environ. Res.*, 2022, **203**, 111819.
149 W.-Q. Chen, L.-Y. Li, L. Li, W.-H. Qiu, L. Tang, L. Xu, K.-J. Xu and M.-H. Wu, *Engineering*, 2019, **5**, 755–767.
150 C. Zhang, J. Zhang, K. Ou, Y. Liu, Z. Guo, X. Chen, G. Cheng and F. Hu, *Colloids Surf., A*, 2021, **615**, 126257.
151 N. M. Mahmoodi, S. Keshavarzi, M. Oveisi, S. Rahimi and B. Hayati, *J. Mol. Liq.*, 2019, **291**, 111333.